SUPPORTING INFORMATION

Synthesis and characterization of dinuclear allenediide bridged hafnocene(IV) complexes

Kevin Lindenau, Edgar Zander, Claas Schünemann, Anke Spannenberg, Maxim V. Andreev, Vladimir V. Burlakov, Fabian Reiß* and Torsten Beweries*

a) Leibniz-Institut für Katalyse e.V., Albert-Einstein-Str. 29a, 18059 Rostock, Germany.

b) Abteilung für Anorganische Chemie, Institut für Chemie, Universität Rostock, Albert-Einstein-Straße 3a, D-18059 Rostock, Germany.

c) A.N. Nesmeyanov Institute of Organoelement Compounds, Russian Academy of Sciences, Vavilov Street 28, 119991 Moscow, Russia

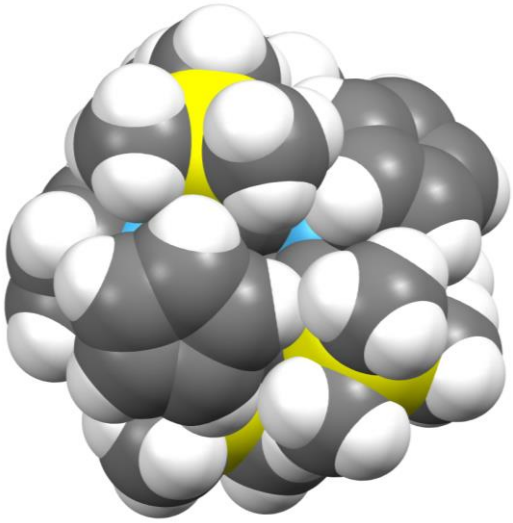

Table of contents

1. Experimental Details S2
2. Details of NMR spectroscopy S5
3. Stability tests / Reactivity tests S28
4. Crystallographic details S38
5. Details of vibrational spectroscopy S41
6. Computational details S44
7. References S47

1. Experimental Details

1.1. General

All manipulations were carried out in an oxygen- and moisture-free argon atmosphere using standard Schlenk and drybox techniques. The solvents were purified with the Grubbs-type column system "Pure Solv MD-5" and dispensed into thick-walled glass Schlenk bombs equipped with Young-type Teflon valve stopcocks. Cp_2HfCl_2 was purchased from MCAT, Me_3SiCl from TCI chemicals and Ph_2PCl from Sigma-Aldrich. Compound **1** and $Cp_2Hf(n\text{-}Bu)_2$ was prepared following literature procedures.[1, 2]

NMR spectra were recorded on Bruker AV300 and AV400 spectrometers. ^{1}H and ^{13}C chemical shifts were referenced to the solvent signal: benzene-d_6 (δ_H = 7.16 ppm, δ_C = 128.06 ppm), toluene-d_8 (δ_H = 2.08 ppm, δ_C = 20.43 ppm), THF-d_8 (δ_H = 3.58 ppm, δ_C = 25.3 ppm).[3]

Raman spectra were recorded on a LabRAM HR 800 Raman Horiba spectrometer equipped with an Olympus BX41 microscope with variable lenses. The samples were excited by different laser sources: 633 nm (17 mW, air cooled), 784 nm Laser diode (100 mW, air-cooled) or 473 nm Ar+ Laser (20 mW, air-cooled). All measurements were carried out at ambient temperature.

IR spectra were recorded on a Bruker Alpha FT-IR, ATR Spectrometer, spectra are not corrected.

MS analysis was done using a Finnigan MAT 95-XP instrument (Thermo-Electron) in CI^+/CI^- mode (isobutene) and for the air stable compounds in EI mode.

CHN analysis was done using a Leco TruSpec elemental analyser. At this point it should be pointed out that in the case of the bimetallic hafnocene complexes we could not obtain satisfactory elemental analysis in most cases. Despite repeated recrystallisation, repeated measurements with and without oxidiser V_2O_5 and modified furnace temperature, we observed up to 20% less carbon content than calculated/expected. This behaviour might be explained by formation of mixed zircon-silicon-carbides (ceramics) in the furnace and therefore the carbon content dramatically decreases.[4]

Melting points are uncorrected and were determined in sealed capillaries under Ar atmosphere using a Mettler-Toledo MP 70.

X-Ray diffraction data were collected on a Bruker Kappa APEX II Duo diffractometer. The structures were solved by direct methods (SHELXS-97)[5] and refined by full-matrix least-squares procedures on F^2 (SHELXL-2014 and SHELXL-2018, resp.).[6] Diamond[7] was used for graphical representations.

All DFT calculations were carried out with the Gaussian 16 package of molecular orbital programs.

1.2. Synthesis of complex 2-Hf

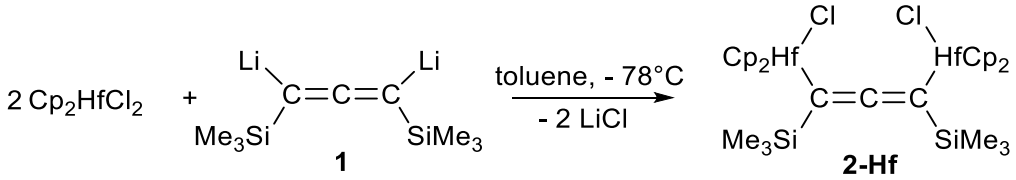

White solids of Cp_2HfCl_2 (300 mg, 0.79 mmol) and **1** (77 mg, 0.40 mmol) were placed in a Schlenk flask in the glove box and dissolved in toluene (10 mL) at - 78 °C. The resulting yellow solution was stirred overnight at -78 °C. A color change to red was observed immediately after addition of $[Li_2(Me_3SiC{=}C{=}CSiMe_3)]$. After filtration at -78 °C another 0.5 eq of $[Li_2(Me_3SiC{=}C{=}CSiMe_3)]$ was added to the solution at room temperature and the mixture was stirred overnight at -78 °C. The yellow solution was filtered off and the filtrate was concentrated in vacuum and stored at -78 °C overnight. Yellow crystals of **2-Hf** could be obtained from toluene at -78 °C but must be separated morphologically from colorless crystals of Cp_2HfCl_2 in the glove box (63mg, 21%).

^{1}H NMR (25 °C, benzene-d_6, 300.2 MHz): δ 6.08 ppm (s, 10H, *Cp*), 6.03 (s, 10H, *Cp*), 0.40 ppm (s, $^2J_{H,Si}$ = 6.3 Hz, 18H, (Si*CH*$_3$)$_3$). **^{13}C NMR** (25 °C, benzene-d_6, 100 MHz): δ 182.8 (C=*C*=C), 113.0 (Cp), 112.6 (Cp), 101.6 (*C*=C=*C*), 3.5 ppm (Si*C*H$_3$). **^{29}Si-inept NMR** (25 °C, benzene-d_6, 79.5 MHz): δ -4.08 (*Si*Me$_3$). **IR** (ATR, cm^{-1}): $\tilde{\nu}$ = 523 (w), 622 (w), 799(vs), 1014 (s), 1238 (s), 1438 (m), 1733 (s), 1768 (s), 1844 (m), 2893 (w), 2949 (w), 3104 (w) cm^{-1} **RAMAN** (632 nm, 10 sec, 8 scans): 131 (m), 147 (s), 166 (w), 263 (s), 292 (w), 318 (vs), 612 (vw), 828 (vw), 852 (vw), 1067 (w), 1129 (ws), 1366 (w), 1441 (w), 3122 (m) cm^{-1}. **MS-CI$^+$** (*isobutene*): *m/z* (%): 835 (25) $[(Cp_2Hf)_2(Me_3SiC_3SiMe_3Cl)]^+$, 799 (20) $[(Cp_2Hf)_2(Me_3SiC_3SiMe_3)]^+$, 669 (31) $[(Cp_2Hf_2Me_3SiC_3SiMe_3]^+$, 492 (100) $[Cp_2HfMe_3SiC_3SiMe_3]^+$, 185 (10) $[Me_3SiC_3SiMe_3]^+$, 73 (8) $[Si(CH_3)_3]^+$. **Mp**: 124 °C (decomp.). **CHN analysis:** calc (%) for $C_{29}H_{38}Si_2Hf_2Cl_2$: C 40.1, H 4.40; Found: C 28.3, H 3.1.

1.3. Synthesis of complex 3-Hf

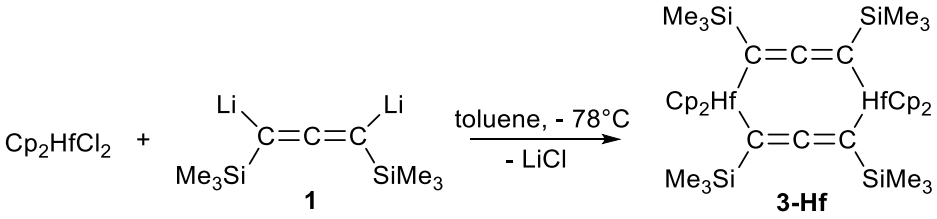

White solids of Cp_2HfCl_2 (151 mg, 0.40 mmol) and **1** (78 mg, 0.40 mmol) were placed in a Schlenk flask in the glove box and dissolved in toluene (10 mL) at - 78 °C. A color change to red was observed immediately. The red solution was stirred overnight at -78 °C. After filtration the solution was concentrated and stored at -78 °C overnight. Orange crystals could be obtained from toluene at -78 °C (136 mg, 90%).

^{1}H NMR (25 °C, benzene-d_6, 300.2 MHz): δ 6.00 (s, 20H, *Cp*). 0.41 ppm (s, $^2J_{H,Si}$ = 6.2 Hz, 18H, (Si*CH*$_3$)$_3$) **^{13}C NMR** (25 °C, benzene-d_6, 75.5 MHz): δ 177.8 (C=*C*=C), 109.7 (Cp), 106.1 (*C*=C=*C*), 3.9 ppm (Si*C*H$_3$). **^{29}Si-inept NMR** (25 °C, benzene-d_6, 79.5 MHz): δ -6.70 ppm (*Si*Me$_3$). **IR** (ATR, cm^{-1}): $\tilde{\nu}$ = 492 (m), 619 (m), 674 (m), 742 (w), 787 (w), 821 (m), 1017 (m), 1239 (s), 1447 (w), 1775 (vs) 1793 (s), 2897 (w), 2948 (w) cm^{-1} **Raman** (633 nm, 20 s, 15 scans): $\tilde{\nu}$ = 297 (w), 315 (w), 370 (m), 513 (vw), 622 (vw), 783 (vw),

795 (vw), 1074 (vw), 1132 (s), 1367 (w), 1439 (w), 1779 (w), 1797 (w), 2894 (m), 2953 (vw), 3111 (w), 3142 (vw) cm^{-1}. **MS-CI$^+$** (*isobutene*): *m/z* (%): 982 (100) $[(Cp_2Hf)_2(Me_3SiC_3SiMe_3)_2]^+$, 917 (23) $[(Cp_2Hf)(CpHf)(Me_3SiC_3SiMe_3)_2]^+$, 185 (17) $[Me_3SiC_3SiMe_3]^+$, 73 (29) $[Si(CH_3)_3]^+$. **Mp**: 320 °C (subl.). **CHN analysis:** calc (%) for $C_{38}H_{56}Si_4Hf_2$: C 46.4, H 5.75; Found: C 46.2, H 5.40.

1.4. Synthesis of Cp_2HfI_2

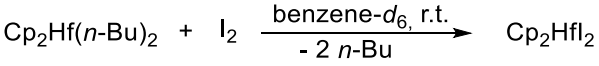

White solid of $Cp_2Hf(n\text{-}Bu)_2$ (25 mg, 0.06 mmol) was placed in a NMR tube in the glove box and dissolved in benzene-d_6 (0.6 mL) at room temperature. An excess of I_2 was added to the reaction mixture and the sample was analysed by NMR spectroscopy. Colourless crystals could be obtained from benzene at room temperature after storing overnight.

^{1}H NMR (25 °C, benzene-d_6, 400.1 MHz): δ 5.86 ppm (s, 10H, *Cp*).[8]

1.5. Synthesis of {$[Ph_2P]_2[C_3(SiMe_3)_2]$} (4-P)

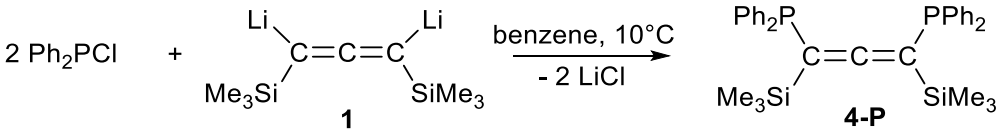

White solid of **1** (250 mg, 1.27 mmol) was placed in a Schlenk flask in the glove box and dissolved in benzene at 10 °C. Neat Ph_2PCl (0.5 mL, 2.73 mmol) was slowly added via a syringe at 10 °C and the mixture was stirred overnight. The colorless solution was filtered and concentrated slowly in a flow of argon. The obtained colorless solid are washed with pentane. Colorless crystals of **4-P** could be obtained from hexane at -78 °C. (233 mg, 77%).

The Raman spectrum could not be measured because the sample heats up due to the irradiation and thus no meaningful spectra can be recorded.

^{1}H NMR (25 °C, benzene-d_6, 400.1 MHz): δ 7.47 ppm (m, 4H, Ar-*H*), 7.26 (m, 4H, Ar-*H*), 7.10 (m, 12H, p, Ar-*H*), 0.13 ppm (s, $^2J_{H,Si}$ = 6.6 Hz, 18H, (Si*CH*$_3$)$_3$). **^{13}C NMR** (25 °C, benzene-d_6, 100.6 MHz): δ 203.6 (C=*C*=C), 138.0 (Ar-*C*), 137.0 (Ar-*C*), 135.1 (Ar-*C*), 134.7 (Ar-*C*), 129.1 (*C*=C=*C*), 128.9 (*C*=C=*C*), 128.4 (Ar-*C*), 80.2 (Ar-*C*), 79.7 (Ar-*C*), 0.4 ppm (Si*C*H$_3$). **^{31}P{^{1}H} NMR** (25 °C, benzene-d_6, 121.5 MHz): δ -10.9 ppm. **^{29}Si-inept NMR** (25 °C, benzene- d_6, 79.49 MHz): δ -0.55 ppm (*Si*Me$_3$), -0.92 ppm (*Si*Me$_3$). **IR** (ATR, cm^{-1}): $\tilde{\nu}$ = 694 (s), 739 (s), 853 (m) 1244 (m), 1432 (m), 1877 (vs), 2893 (vw), 2955 (w), 3046 (vw), 3069 (vw) cm^{-1}. **MS-CI$^+$** (*isobutene*): *m/z* (%): 553 (100) {$[Ph_2P]_2[C_3(SiMe_3)_2]$}. **Mp**: 108 °C (decomp.). **CHN analysis:** calc (%) for $C_{33}H_{38}P_2Si_2$: C 71.7, H 6.93; Found: C 71.6, H 7.05.

2. Details of NMR spectroscopy

2.1. NMR spectra of complex 2-Hf

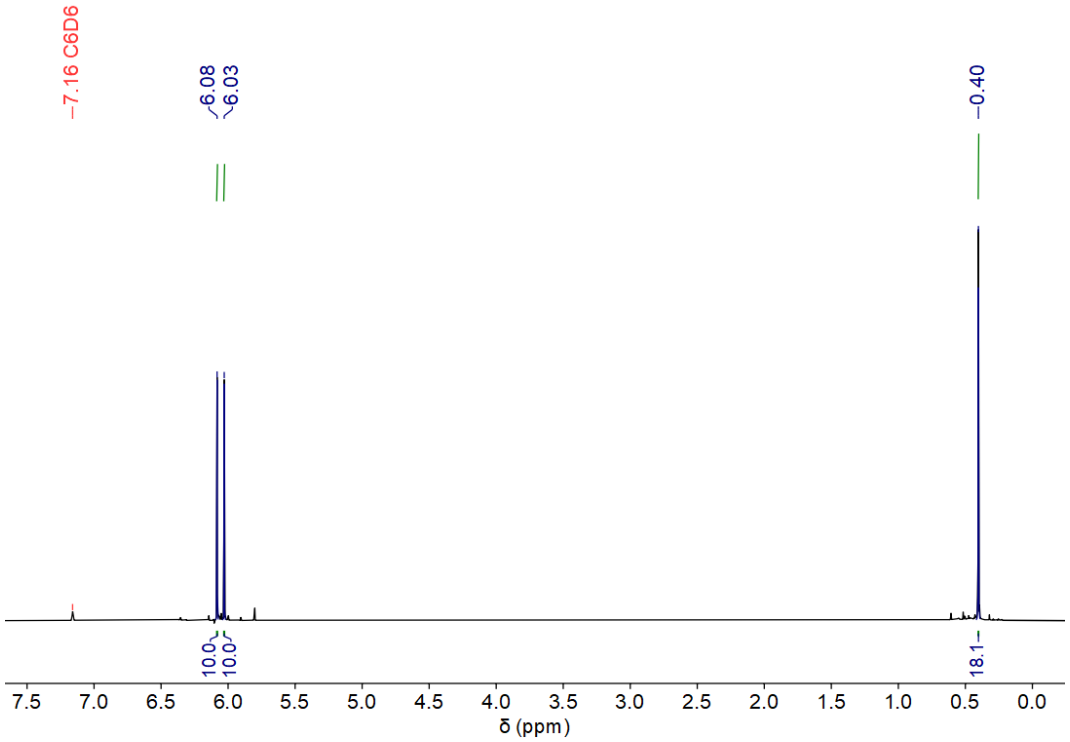

Figure S 1. ^{1}H NMR spectrum of **2-Hf** (25 °C, benzene-d_6, 300.13 MHz).

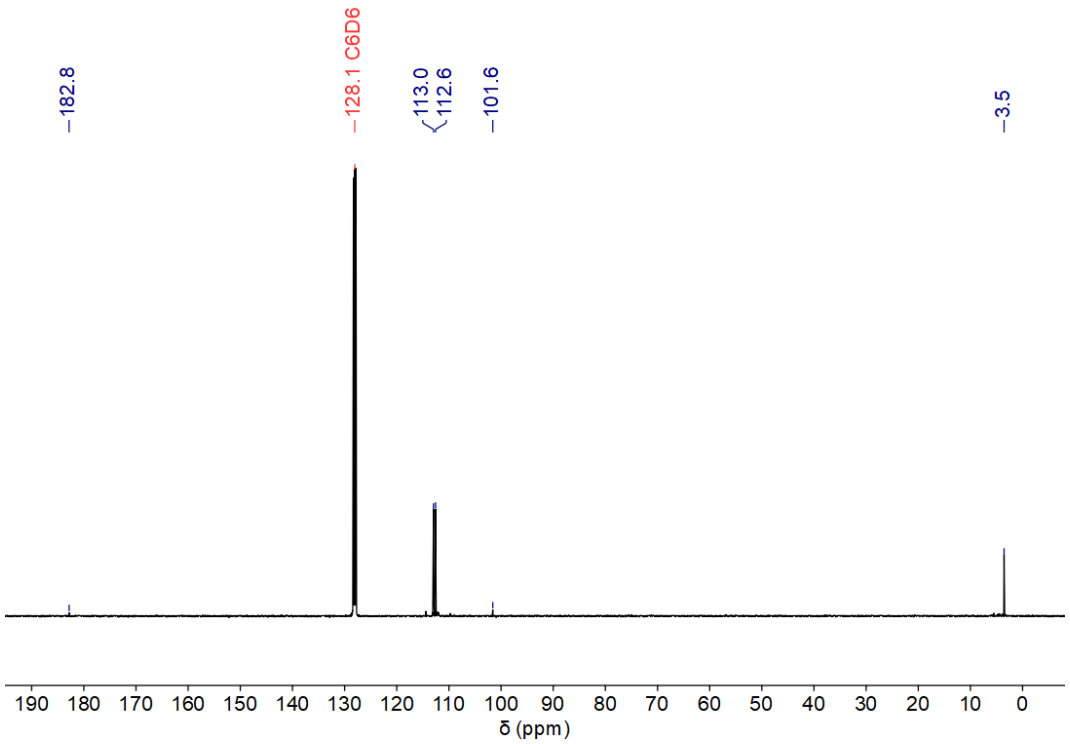

Figure S 2. ^{13}C NMR spectrum of **2-Hf** (25 °C, benzene-d_6, 100.63 MHz).

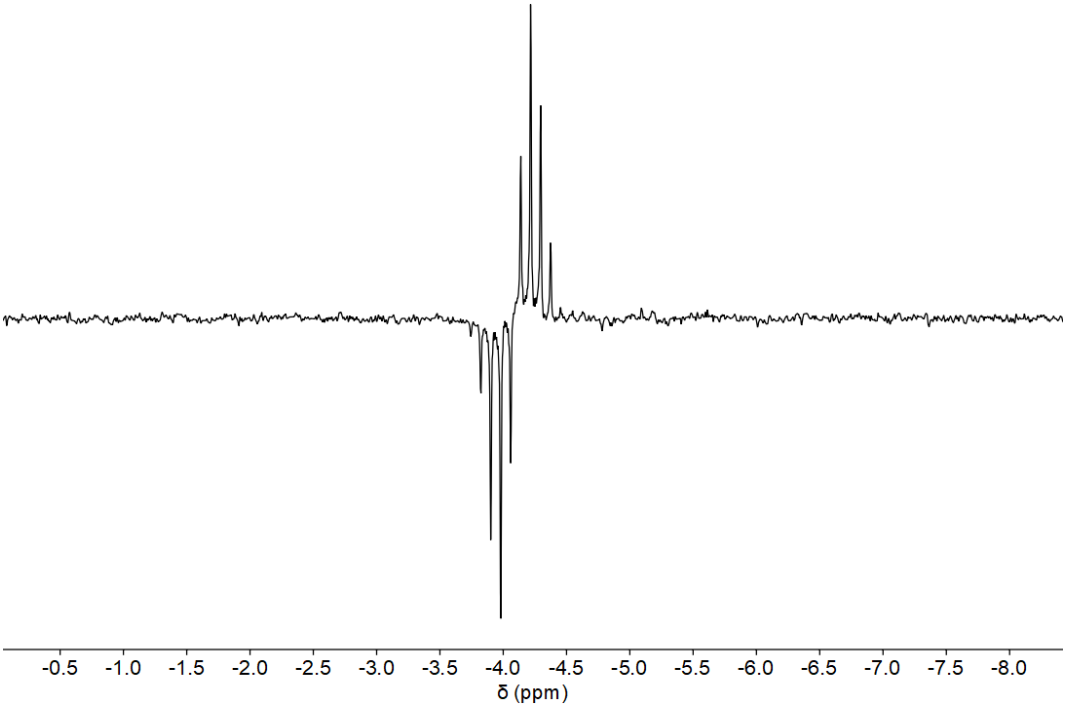

Figure S 3. ^{29}Si INEPT NMR spectrum of **2-Hf** (25 °C, benzene-d_6, 79.5 MHz).

2.2. NMR spectra of complex 3-Hf

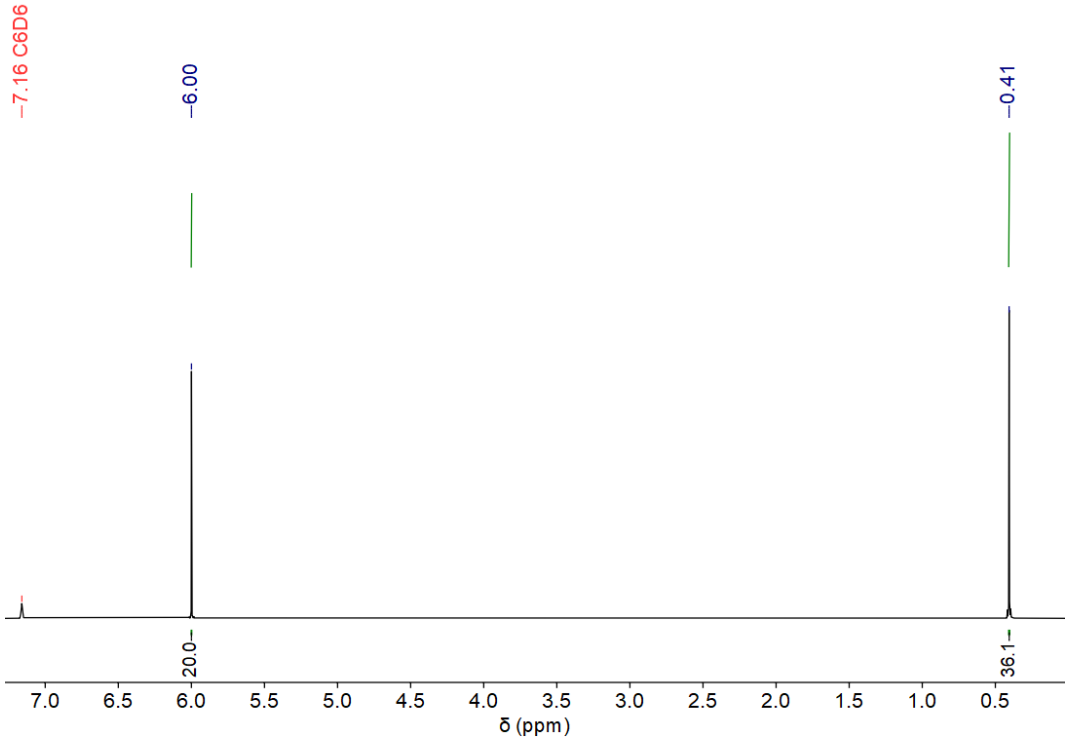

Figure S 4. ^{1}H NMR spectrum of **3-Hf** (25 °C, benzene-d_6, 300.13 MHz).

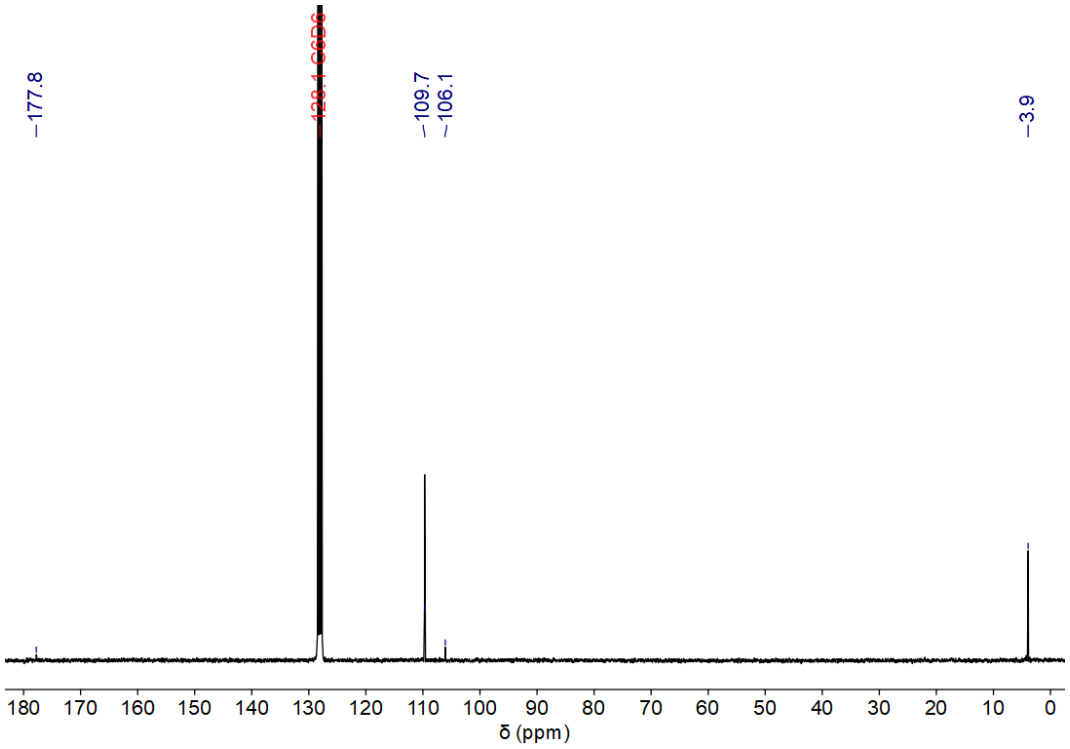

Figure S 5. ^{13}C NMR spectrum of **3-Hf** (25 °C, benzene-d_6, 100.63 MHz).

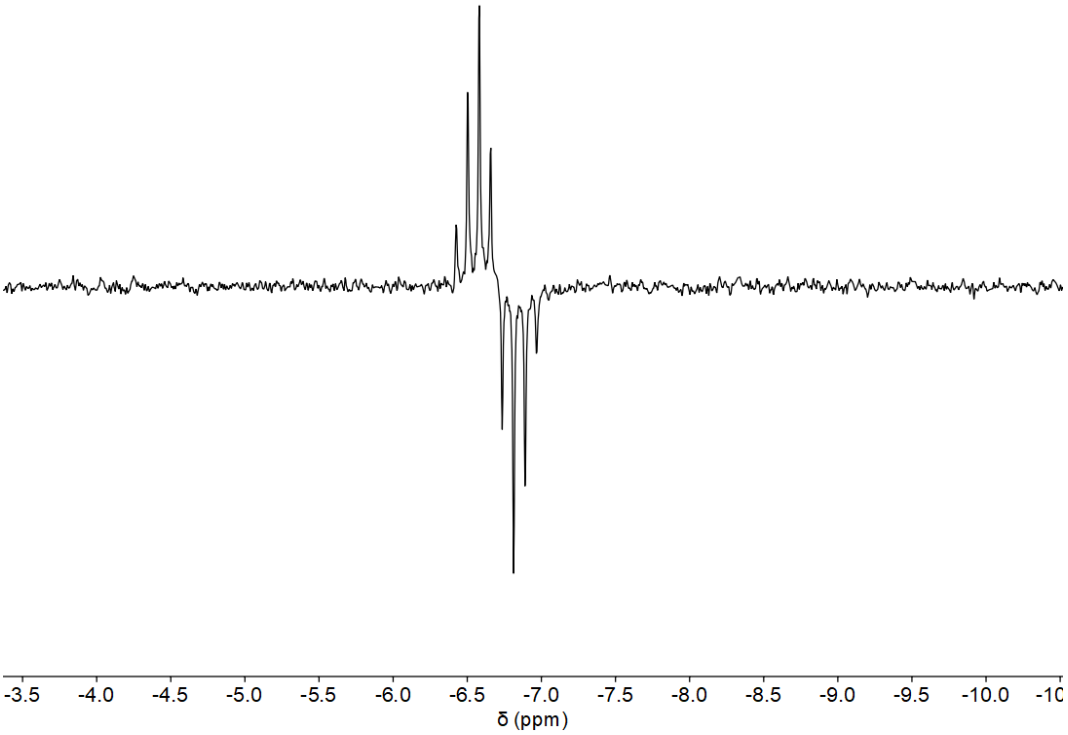

Figure S 6. ^{29}Si INEPT NMR spectrum of **3-Hf** (25 °C, benzene-d_6, 79.49 MHz).

2.3. NMR spectra of {[Ph_2P]$_2$[$C_3(SiMe_3)_2$]} (4-P)

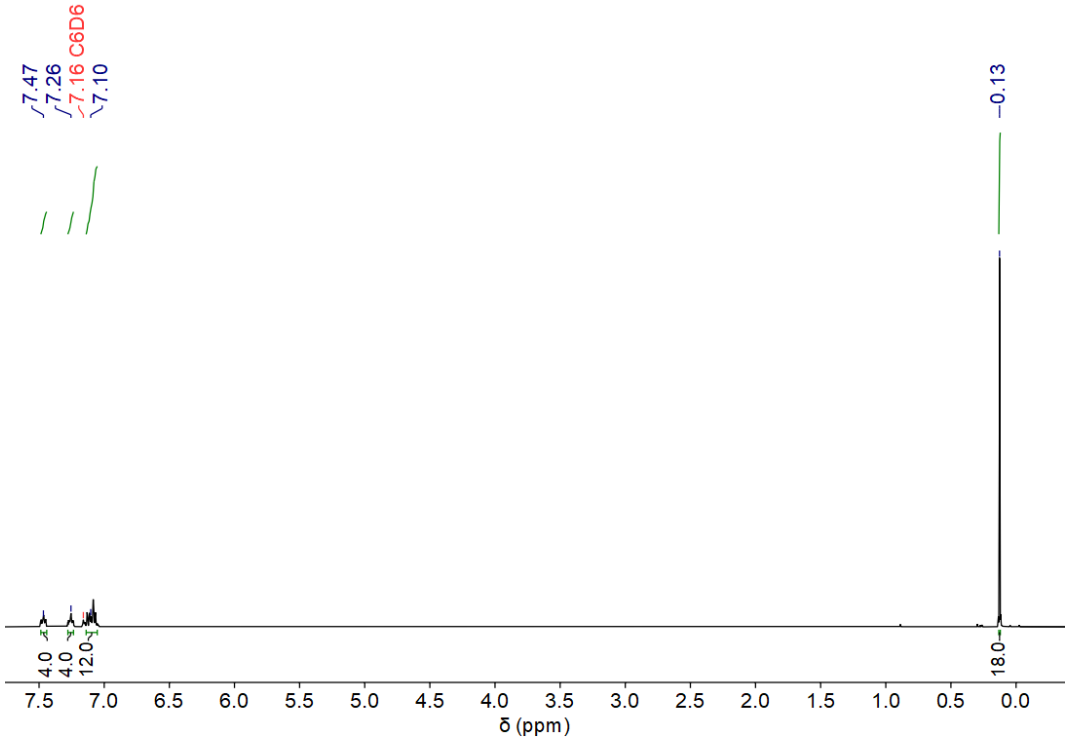

Figure S 7. ^{1}H NMR spectrum of **4-P** (25 °C, benzene-d_6, 400.13 MHz).

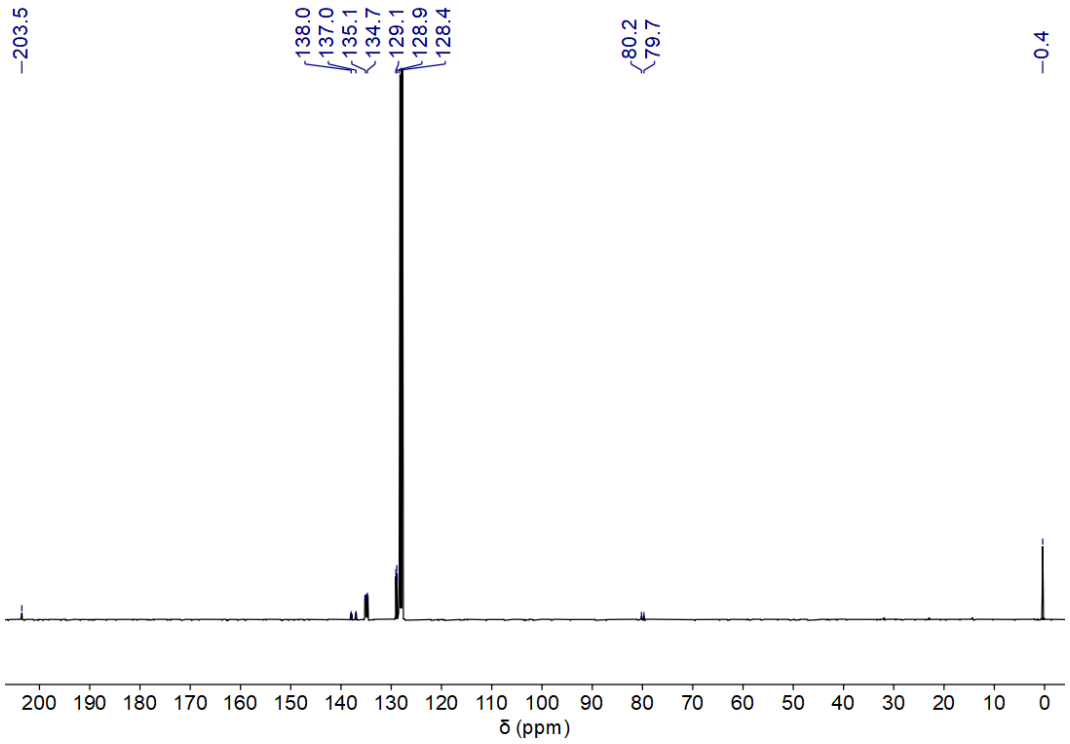

Figure S 8. ^{13}C NMR spectrum of **4-P** (25 °C, benzene-d_6, 100.63 MHz).

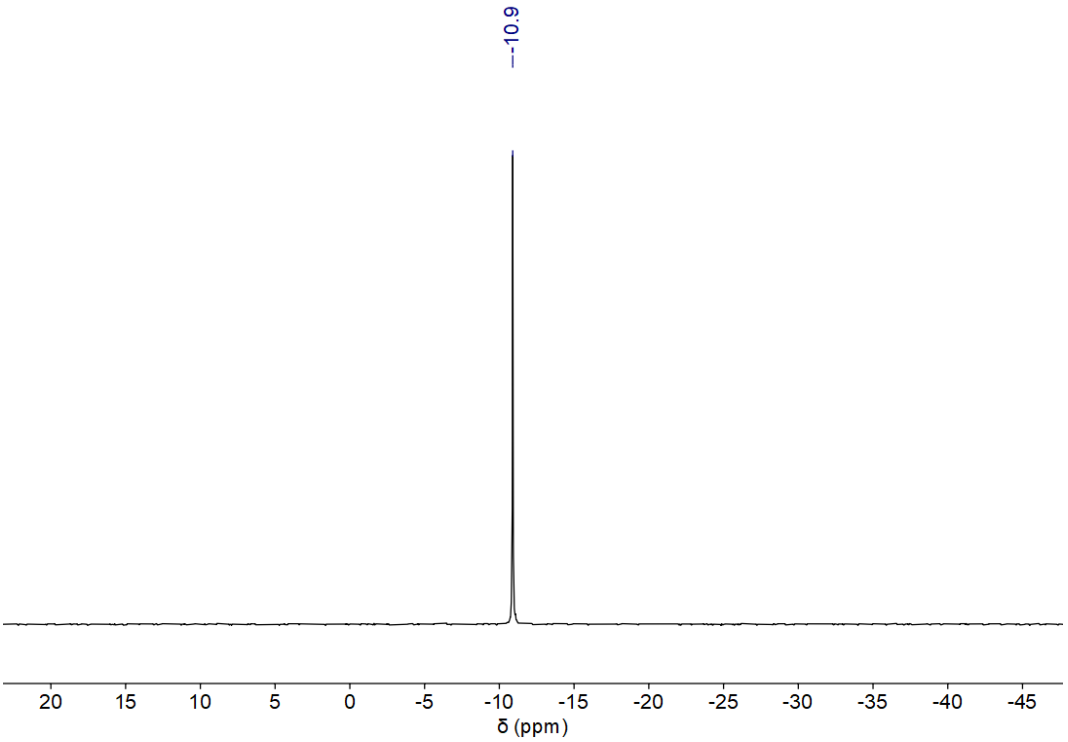

Figure S 9. $^{31}P\{^{1}H\}$ NMR spectrum of **4-P** (25 °C, benzene-d_6, 121.50 MHz).

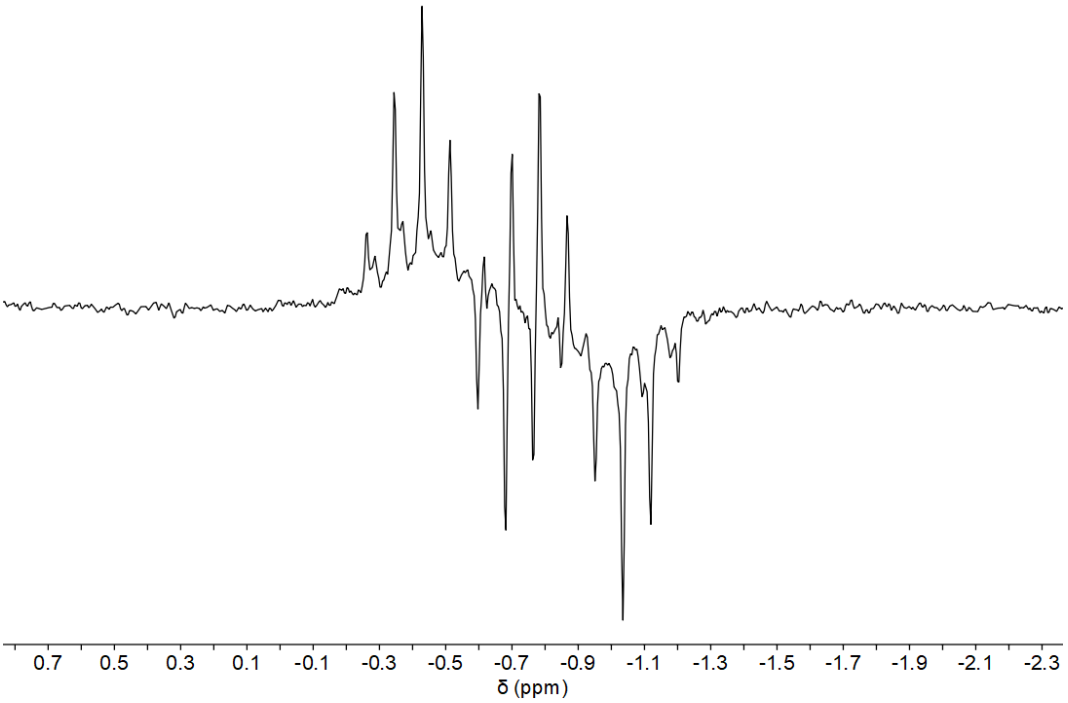

Figure S 10. ^{29}Si INEPT NMR spectrum of **4-P** (25 °C, benzene-d_6, 79.49 MHz).

2.4. NMR spectra of synthesis of 2-Hf in THF

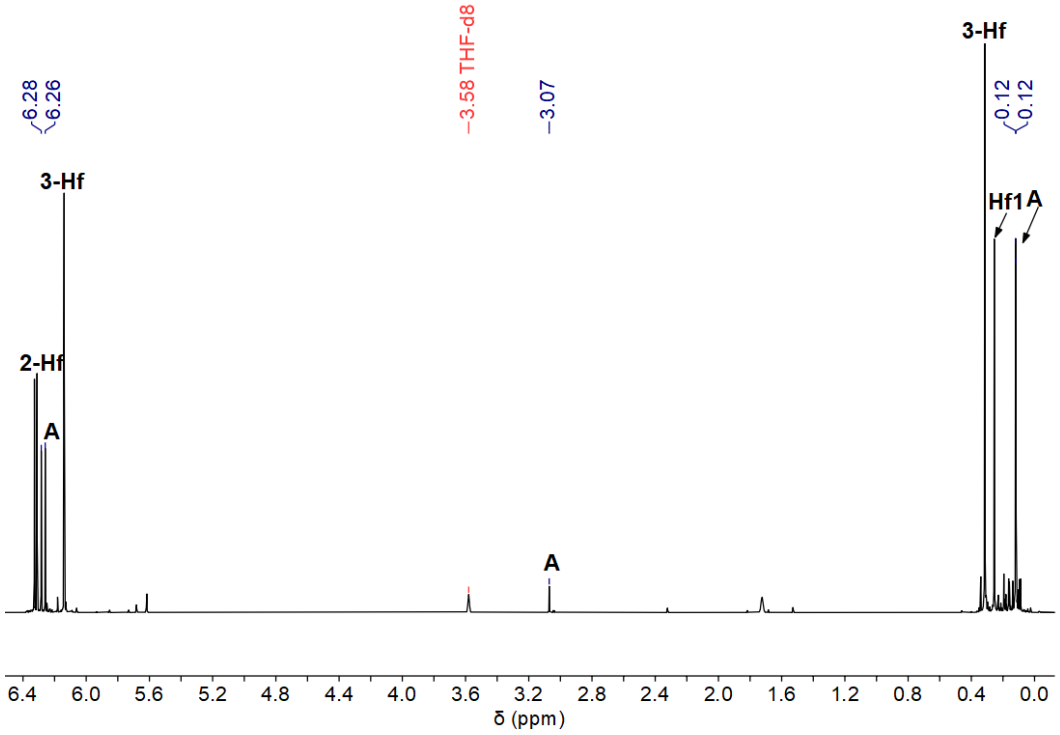

Figure S 11. ^{1}H NMR spectrum of the synthesis of complex **2-Hf** in THF. Conditions: room temperature, THF, 0.05 mmol Cp_2HfCl_2, 0.03 mmol $Li_2[C_3(SiMe_3)_2]$ (25 °C, THF-d_8, 300.20 MHz).

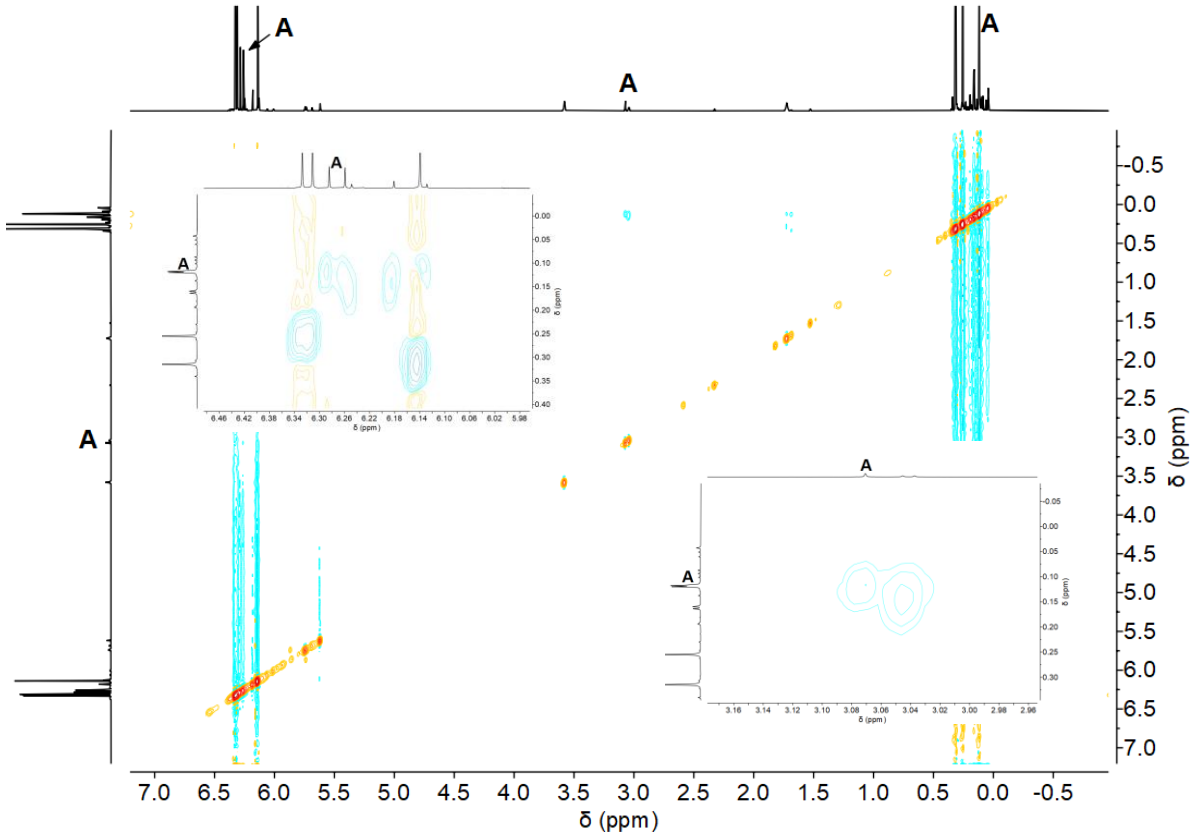

Figure S 12. ^{1}H-^{1}H NOESY NMR spectrum of the synthesis of complex **2-Hf** in THF. Conditions: room temperature, THF, 0.05 mmol Cp_2HfCl_2, 0.03 mmol $Li_2[C_3(SiMe_3)_2]$ (25 °C, THF-d_8, 400.13 MHz).

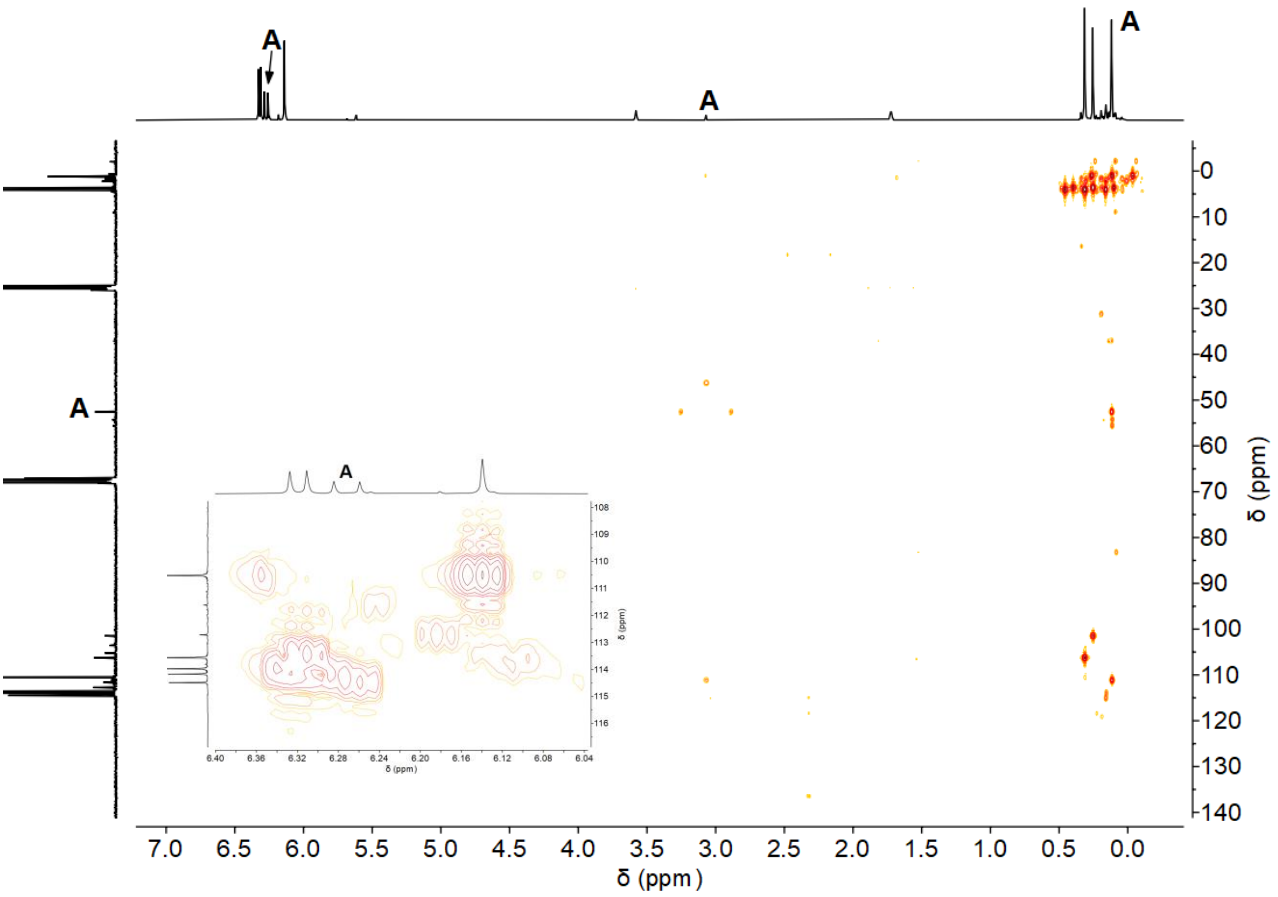

Figure S 13. ^{1}H-^{13}C HMBC NMR spectrum of the synthesis of complex **2-Hf** in THF. Conditions: room temperature, THF, 0.05 mmol Cp_2HfCl_2, 0.03 mmol $Li_2[C_3(SiMe_3)_2]$ (25 °C, THF-d_8, 400.14, 100.62 MHz). The signals at the high-frequency end of the carbon spectrum appear folded in the F1 direction, specifically: 193.9 ppm is detected at 46.0 ppm, 184.6 ppm at 36.7 ppm, and 178.3 ppm at 30.7 ppm (see original ^{13}C spectrum Figure S 14 Top). The true signal position can be calculated from the observed frequency and the limits of the spectral range, and vice versa. Furthermore, we confirmed that the proton which resonates at 3.07 ppm in the ^{1}H NMR is directly connected to the carbon atom which resonates at 52.6 ppm due to the correlation of the ^{13}C satellites in this measurement ($^{1}J_{CH}$ = 146 Hz).

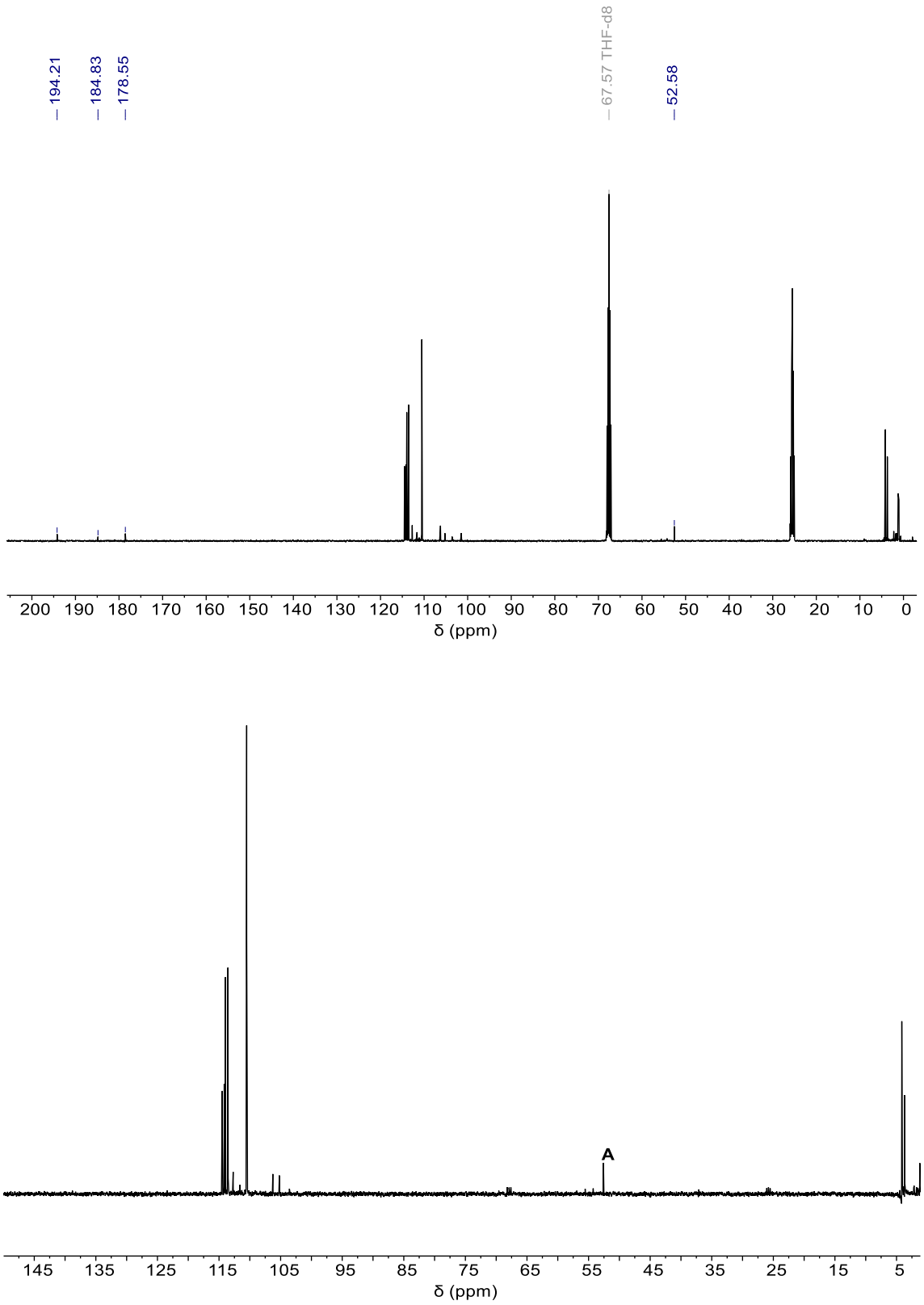

Figure S 14. ^{13}C NMR spectrum (25 °C, THF-d_8, 100.63 MHz, top) and ^{13}C DEPT NMR spectrum of the synthesis of complex **2-Hf** in THF (bottom). Conditions: room temperature, THF, 0.05 mmol Cp_2HfCl_2, 0.03 mmol $Li_2[C_3(SiMe_3)_2]$ (25 °C, THF-d_8, 75.49 MHz). The DEPT spectrum confirms the signal at 52.6 ppm as a resonance due to a CH Group, the direct correlation of this C atom to the signal at 3.07 ppm in the ^1H NMR was detected in the ^1H-^{13}C HMBC measurement (Figure S 13).

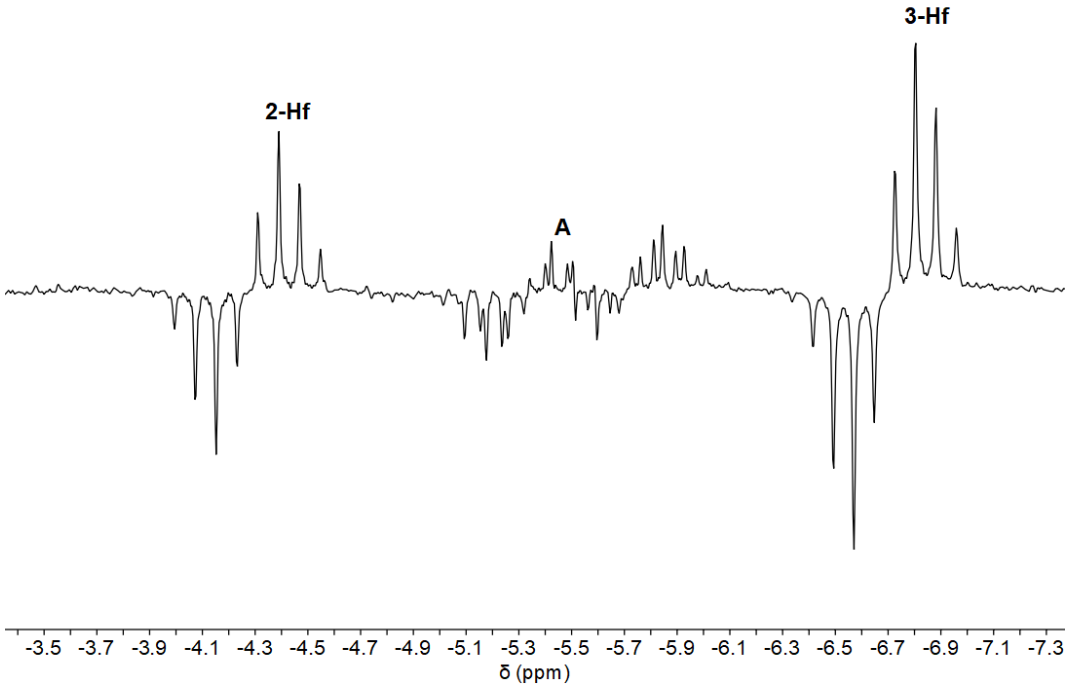

Figure S 15. ^{29}Si INEPT NMR spectrum of the synthesis of complex **2-Hf** in THF. Conditions: room temperature, THF, 0.05 mmol Cp_2HfCl_2, 0.03 mmol $Li_2[C_3(SiMe_3)_2]$ (25 °C, THF-d_8, 79.49 MHz).

2.5. NMR spectra of the synthesis of 2-Hf in different solvents

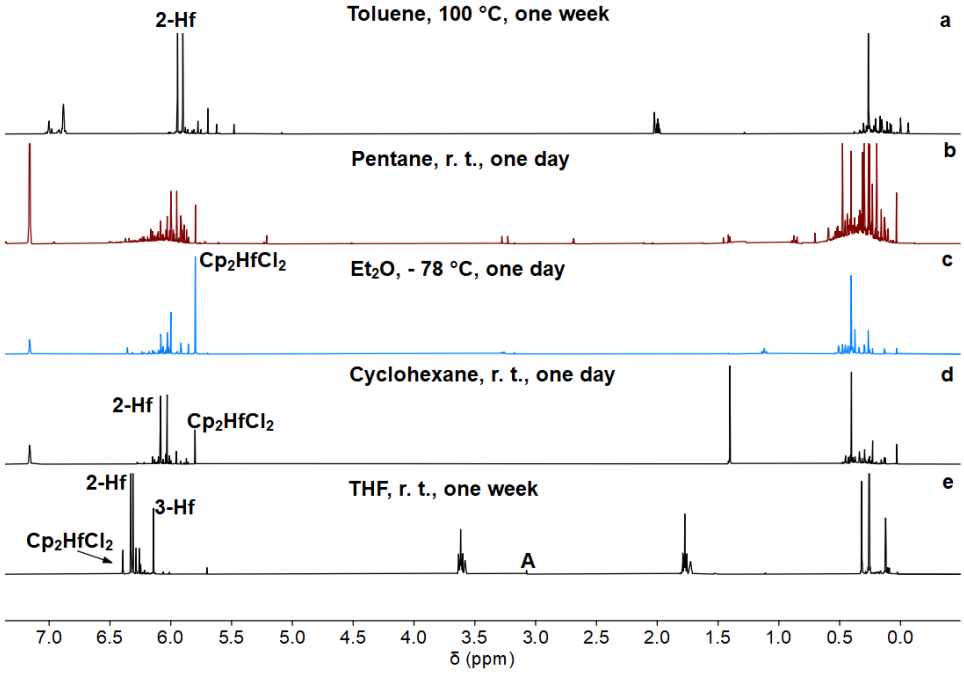

Figure S 16. Comparison of ^{1}H NMR spectra of the synthesis of **2-Hf**.

Conditions: a) solvent 10 mL, 0.36 mmol Cp_2HfCl_2, 0.20 mmol $Li_2[C_3(SiMe_3)_2]$ in toluene (25 °C, toluene-d_8, 300.20 MHz), b) 0.27 mmol Cp_2HfCl_2, 0.14 mmol $Li_2[C_3(SiMe_3)_2]$ in pentane, (25 °C, benzene-d_6, 300.20 MHz), c) 0.27 mmol Cp_2HfCl_2, 0.14 mmol $Li_2[C_3(SiMe_3)_2]$ in Et_2O (25 °C, toluene-d_8, 300.20 MHz), d) 0.36 mmol Cp_2HfCl_2, 0.20 mmol $Li_2[C_3(SiMe_3)_2]$ in cyclohexane (25 °C, benzene-d_6, 300.20 MHz), e) 0.05 mmol Cp_2HfCl_2, 0.03 mmol $Li_2[C_3(SiMe_3)_2]$ in THF (25 °C, THF-d_8, 300.20 MHz).

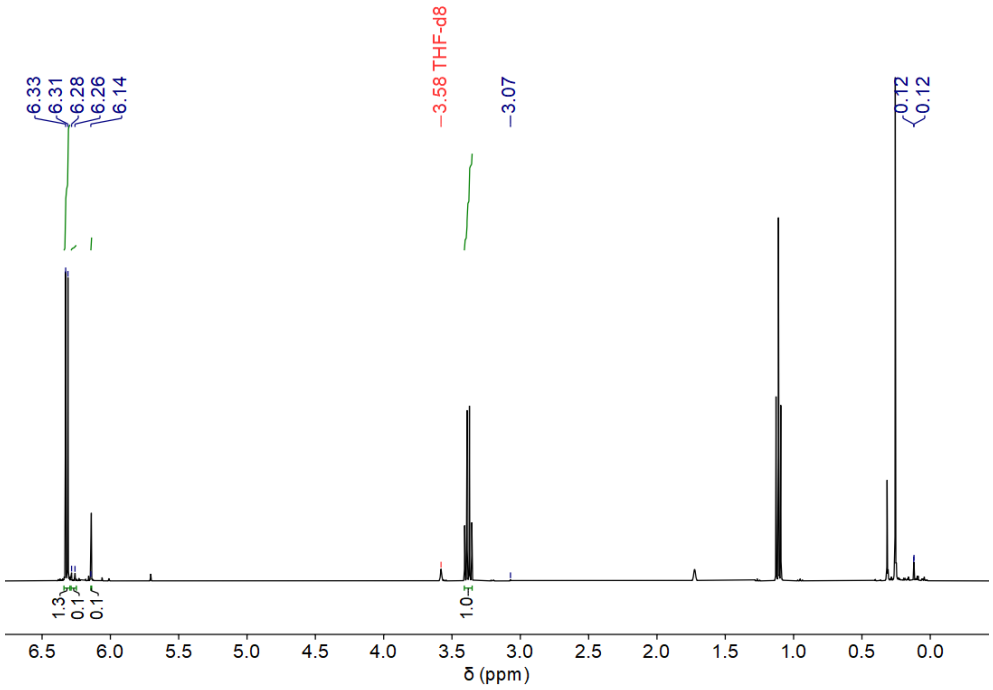

Figure S 17. ^{1}H NMR spectrum of the synthesis of complex **2-Hf** in THF with Et_2O as internal standard. Conditions: room temperature, 0.6 mL THF-d_8, 0.05 mmol Cp_2HfCl_2, 0.03 mmol $Li_2[C_3(SiMe_3)_2]$ 0.105 mmol Et_2O (25 °C, THF-d_8, 300.20 MHz). Using 0.105 mmol of diethyl ether as internal standard a mass distribution of 83% of **2-Hf**, 9% of **3-Hf** and 7% of **A** is observed. The calculation was done based on integral ratios of 1.30 **2-Hf**, 0.13 **3-Hf** and 0.05 for **A.**

2.6. NMR spectra of time-resolved experiments

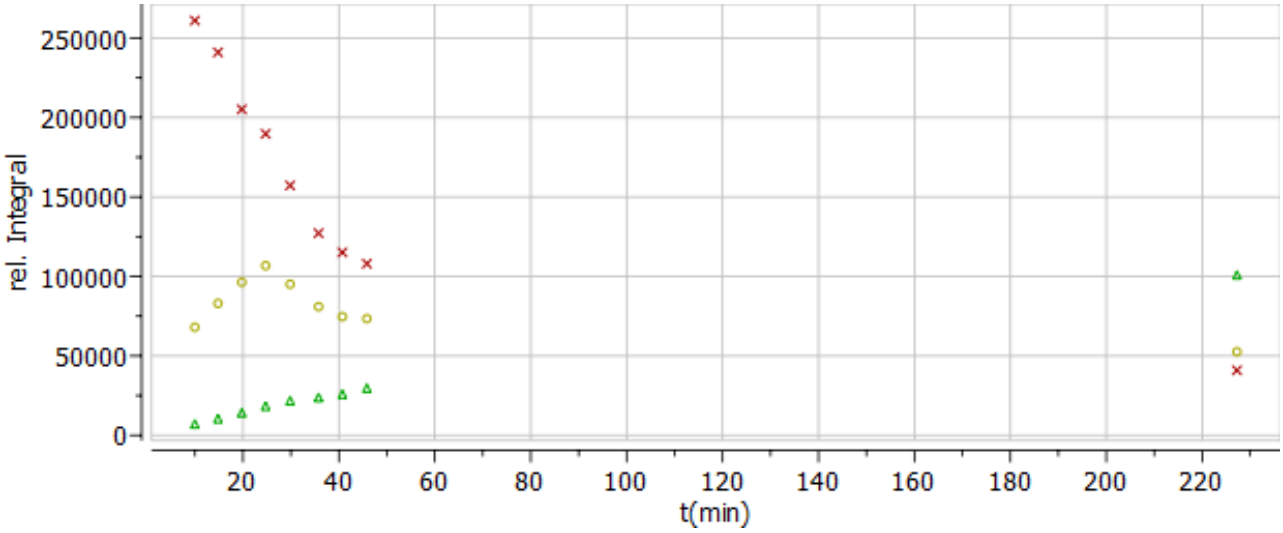

Figure S 18. Concentration time diagram extracted from Figure 3. After 45 min, the reaction was interrupted for a ^{1}H-^{1}H NOESY measurement and resumed at 225 min for the final measurement. For **B**, only the signal at 6.15 ppm was used for simplification (6.09 ppm for **2-Hf**) (25 °C, benzene-d_6, 400.13 MHz, red **Cp_2HfCl_2**, yellow **B** and green **2-Hf**).

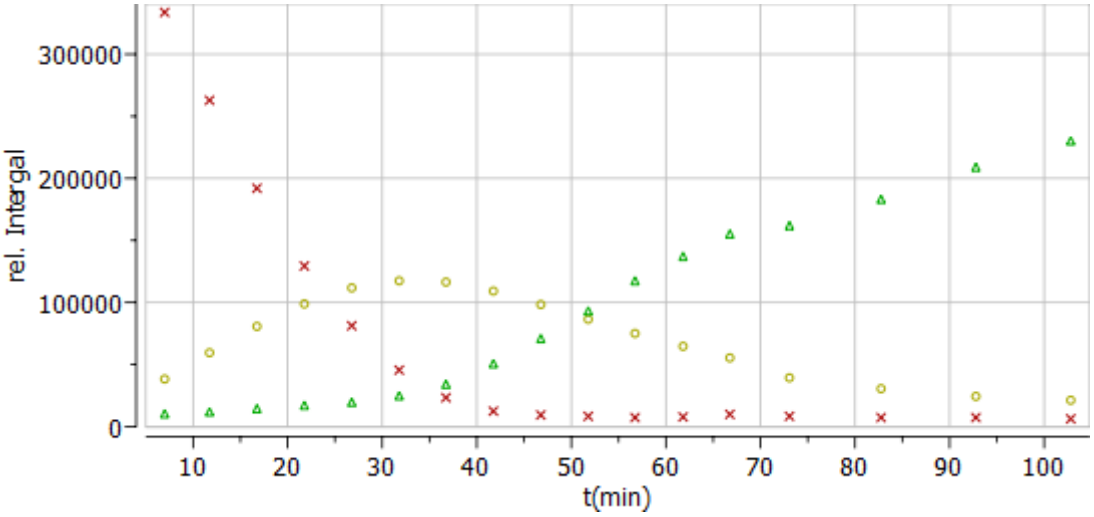

Figure S 19. Concentration time diagram extracted from data Figure S19. For **B**, only the signal at 6.15 ppm was used for simplification (25 °C, benzene-d_6, 400.13 MHz, red **Cp_2HfCl_2**, yellow **B** and green **3-Hf**).

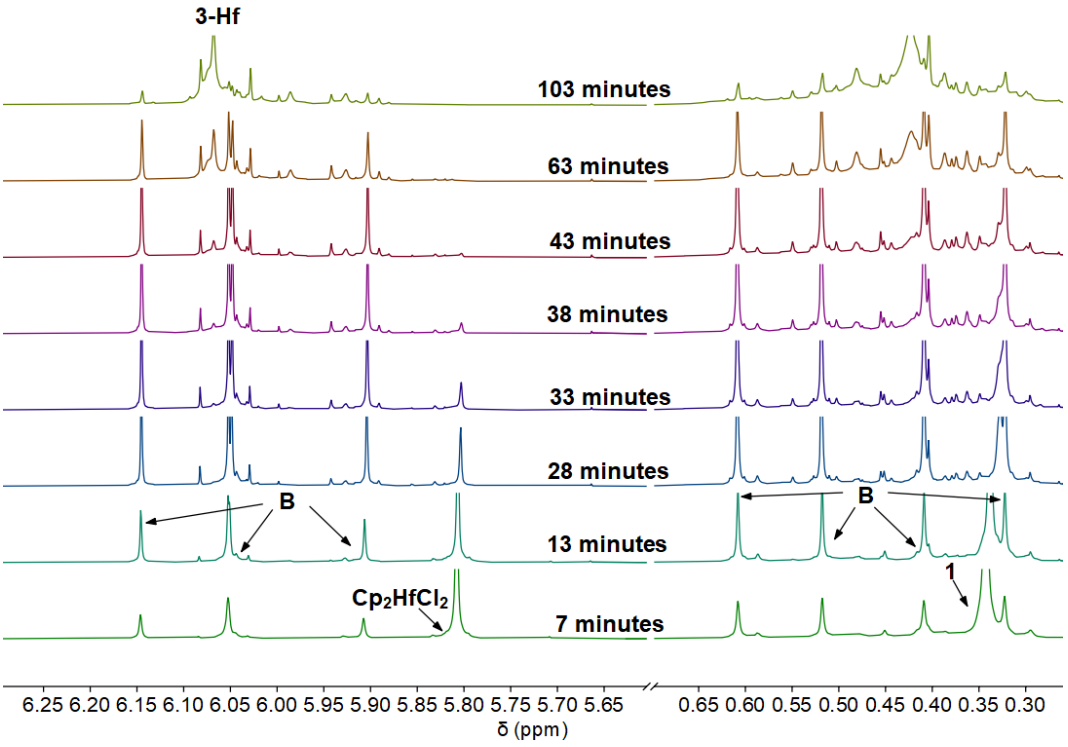

Figure S 20. Time-resolved ^{1}H NMR spectra of the synthesis of complex **3-Hf** (25 °C, benzene-d_6, 400.13 MHz). Conditions: room temperature, benzene, 0.05 mmol Cp_2HfCl_2, 0.03 mmol $Li_2[C_3(SiMe_3)_2]$.

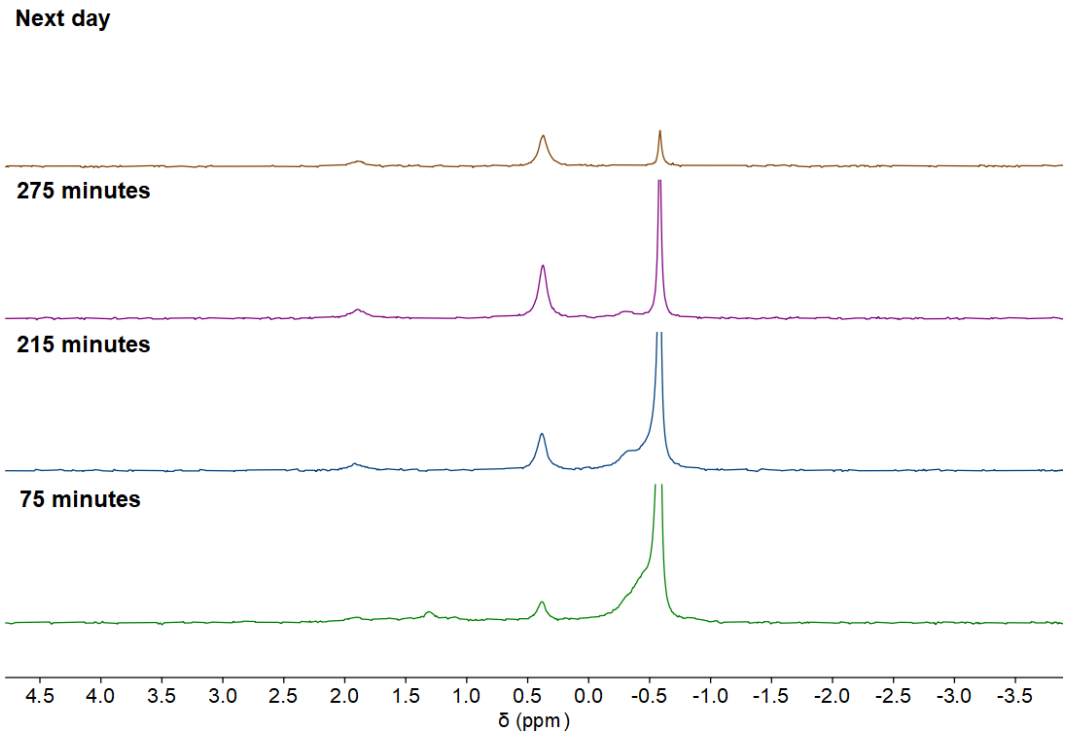

Figure S 21. Time resolved ^{7}Li NMR spectra of the synthesis of complex **2-Hf** (25 °C, benzene-d_6, 400.13 MHz). Conditions: room temperature, benzene, 0.05 mmol Cp_2HfCl_2, 0.03 mmol $Li_2[C_3(SiMe_3)_2]$.

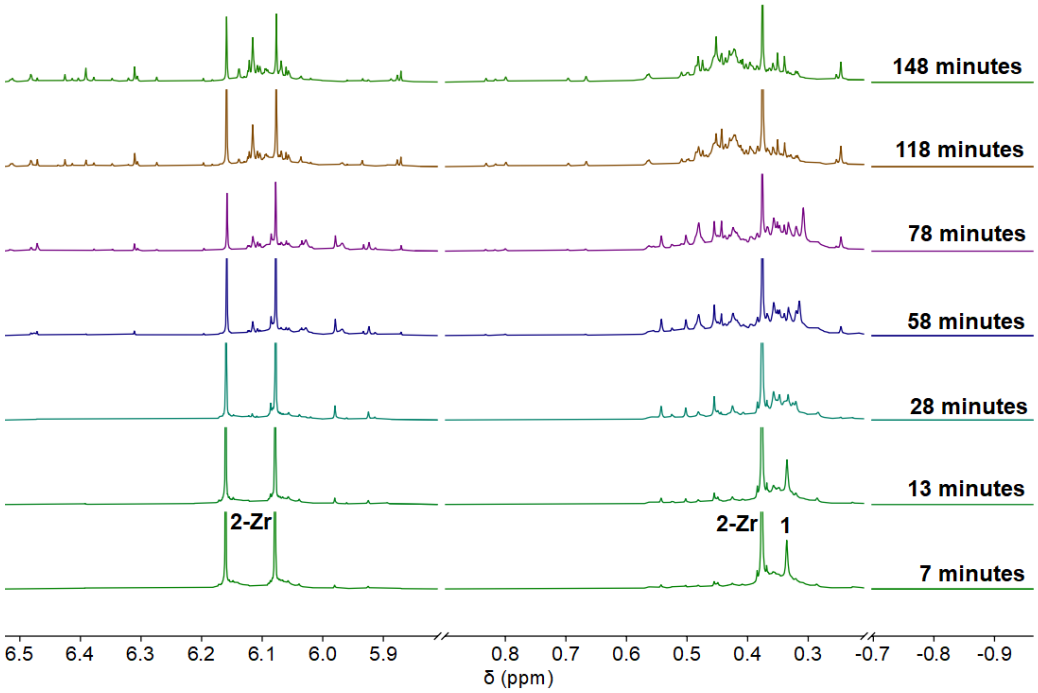

Figure S 22. Time resolved ^{1}H NMR spectra of the synthesis of complex **2-Zr** (25 °C, benzene-d_6, 400.13 MHz). Conditions: room temperature, benzene, 0.14 mmol Cp_2ZrCl_2, 0.07 mmol $Li_2[C_3(SiMe_3)_2]$.

2.7. NMR spectra of the unknown intermediate “B”

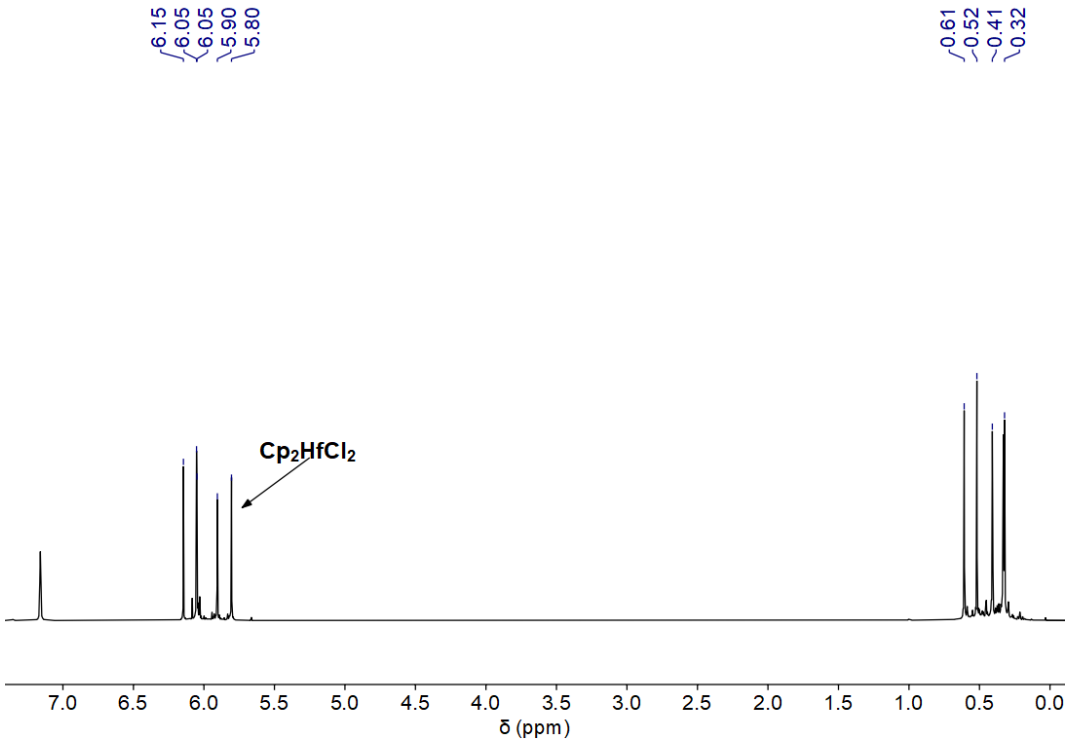

Figure S 23. ^{1}H NMR spectrum of **B** (25 °C, benzene-d_6, 400.20 MHz).

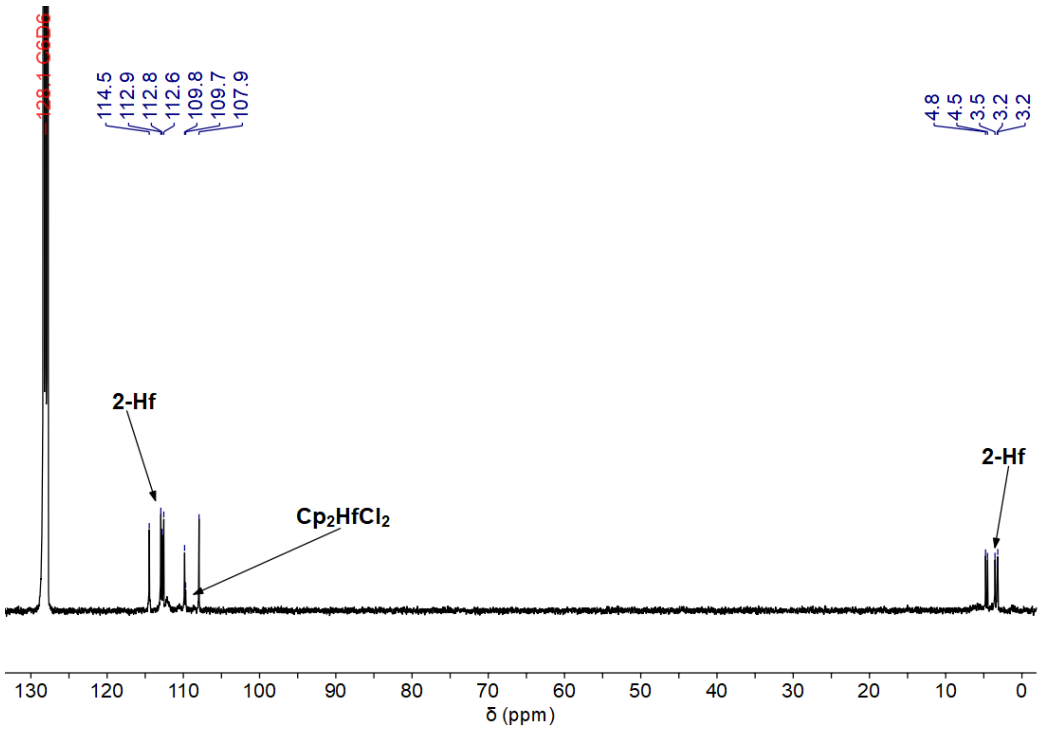

Figure S 24. ^{13}C NMR spectrum of **B** (25 °C, benzene-d_6, 100.63 MHz).

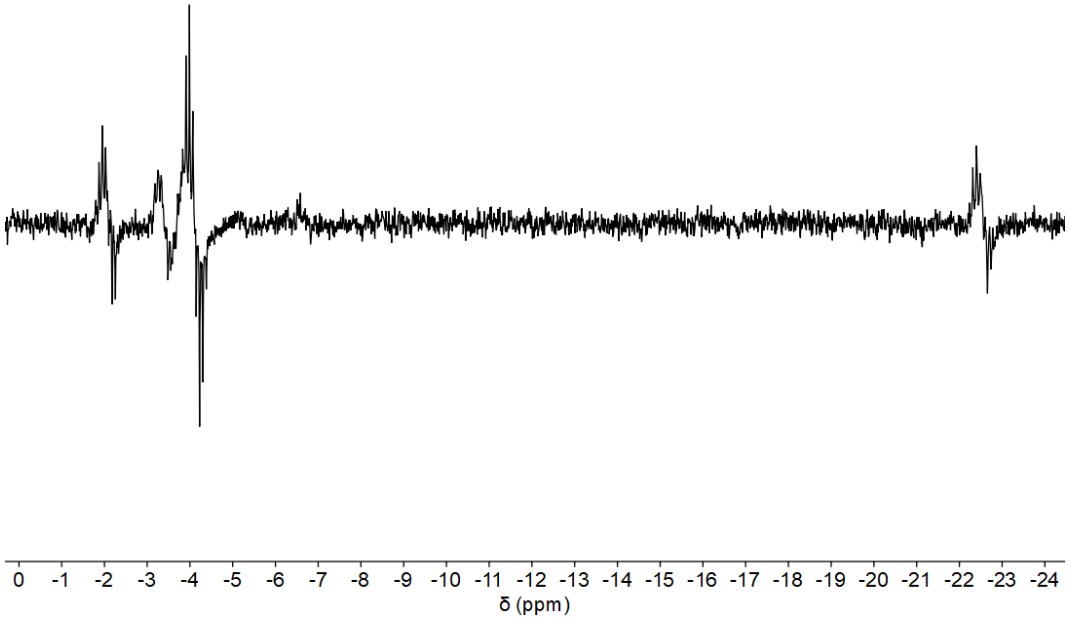

Figure S 25. ^{29}Si INEPT NMR spectrum of **B** (25 °C, benzene-d_6, 79.49 MHz).

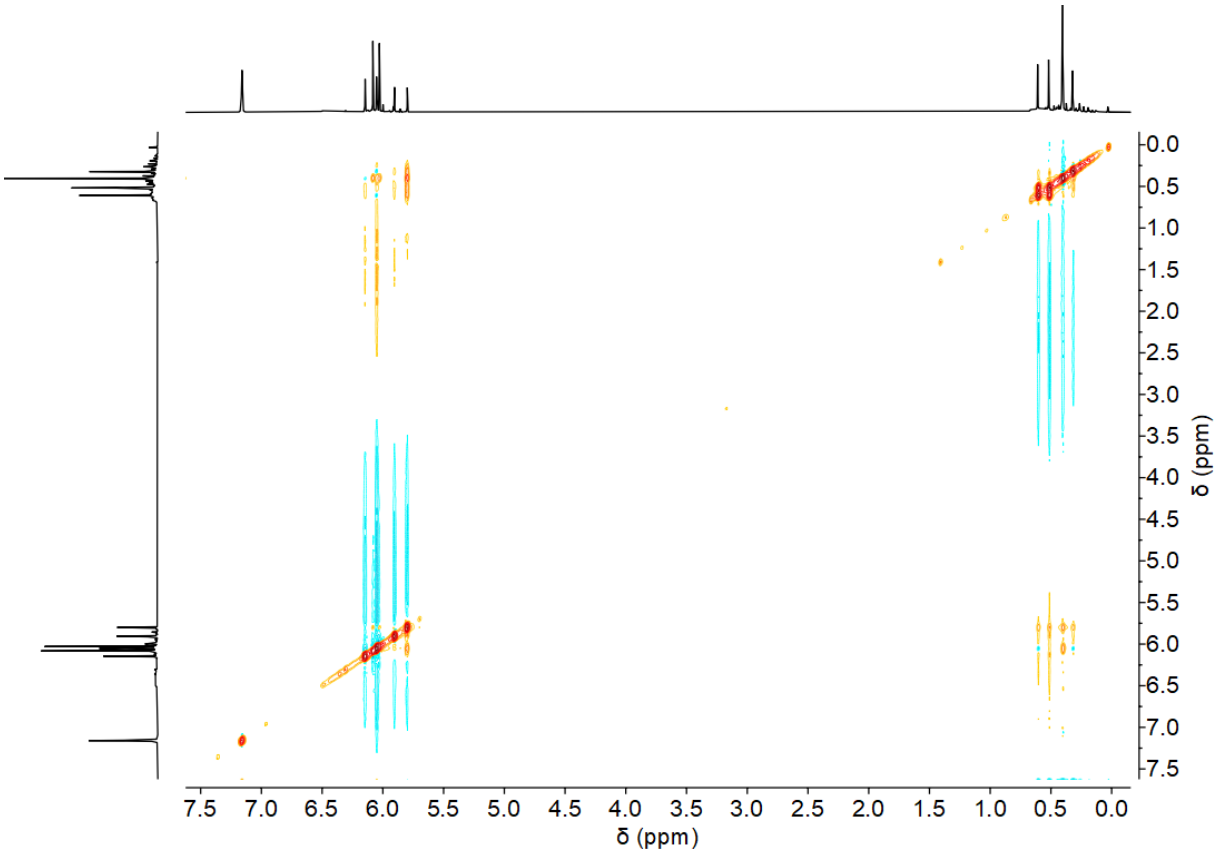

Figure S 26. ^{1}H-^{1}H NOESY NMR spectrum of **B** (25 °C, benzene-d_6, 400.20 MHz).

2.8. NMR spectrum of the synthesis of 2-Hf with 4 eq of 1

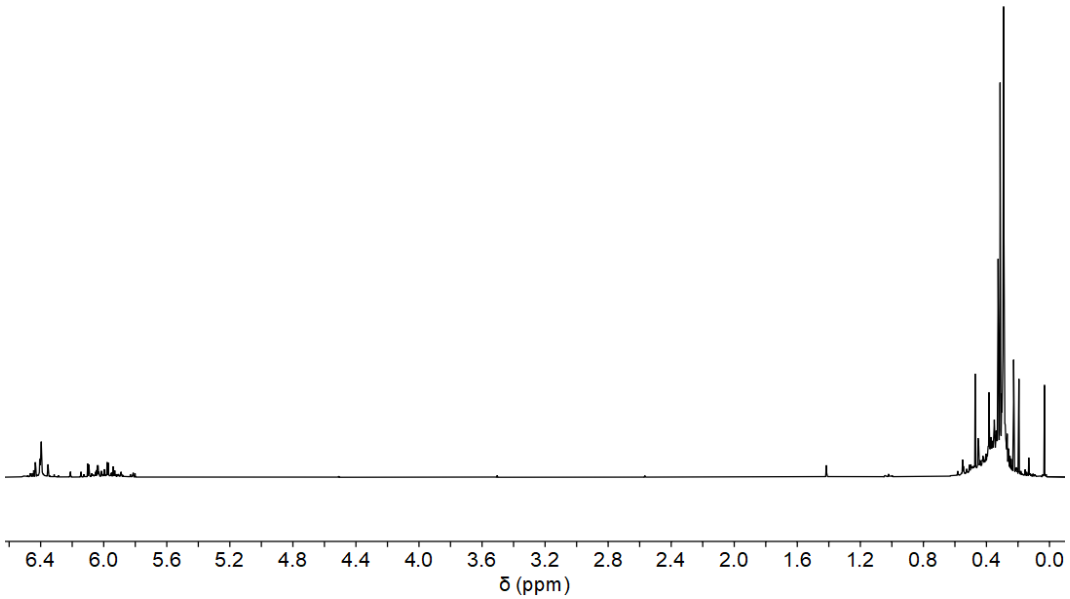

Figure S 27. ^{1}H NMR spectrum of the synthesis of complex **2-Hf** (25 °C, benzene-d_6, 300.20 MHz). Conditions: room temperature, benzene, 0.01 mmol Cp_2HfCl_2, 0.05 mmol $Li_2[C_3(SiMe_3)_2]$.

2.9. NMR spectrum of the synthesis of 2-Hf with 4 eq of Cp_2HfCl_2

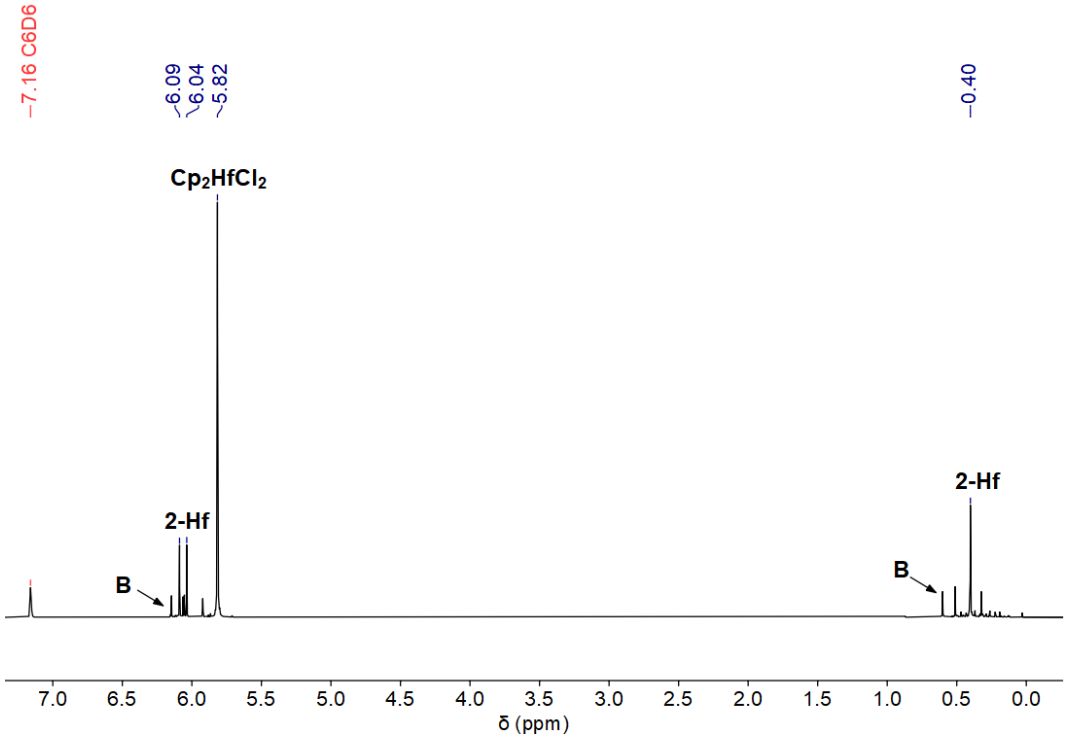

Figure S 28. ^{1}H NMR spectrum of the synthesis of complex **2-Hf** (25 °C, benzene-d_6, 300.20 MHz). Conditions: room temperature, benzene, 0.07 mmol Cp_2HfCl_2, 0.02 mmol $Li_2[C_3(SiMe_3)_2]$.

2.10. NMR spectrum of Cp_2HfICl ligand exchange reaction

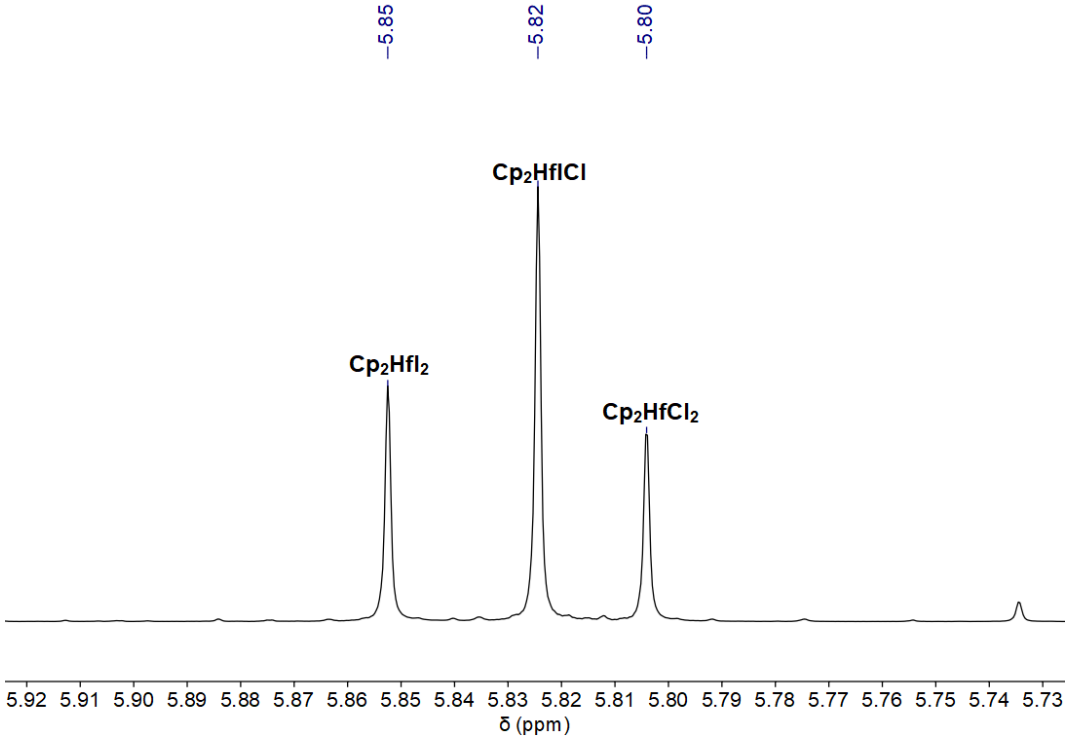

Figure S 29. ^{1}H NMR spectrum of ligand exchange experiment (25 °C, benzene-d_6, 400.13 MHz). Conditions: room temperature, benzene, 0.04 mmol Cp_2HfCl_2, 0.04 mmol Cp_2HfI_2.

2.11. NMR spectra of derivatization experiments

2.11.1. NMR spectrum of the reaction of Cp_2HfCl_2 with $Li_2[C_3(SiMe_3)_2]$ and addition of tetrakisoxacyclododecane (12-C-4)

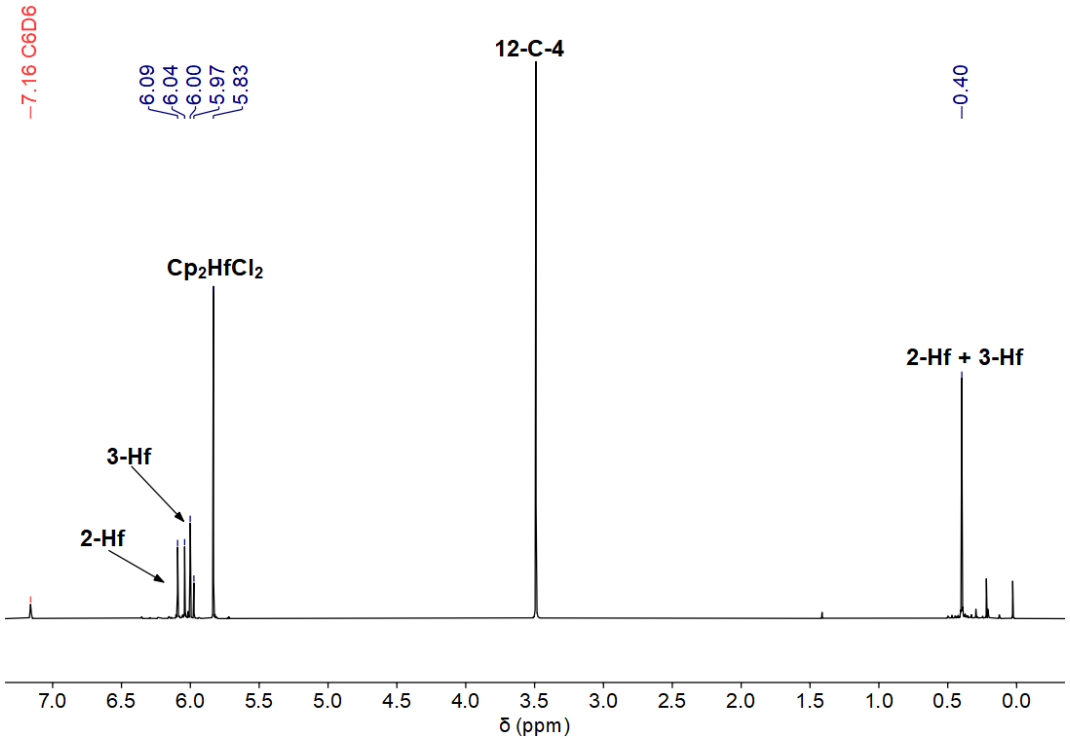

Figure S 30. ^{1}H NMR spectrum of a derivatization experiment with 12-C-4 (25 °C, benzene-d_6, 400.13 MHz). Conditions: room temperature, benzene, 0.10 mmol Cp_2HfCl_2, 0.05 mmol $Li_2[C_3(SiMe_3)_2]$, 0.10 mmol 12-C-4.

2.11.2. NMR spectrum of the reaction of Cp_2HfCl_2 with $Li_2[C_3(SiMe_3)_2]$ and addition of Ph_2PCl

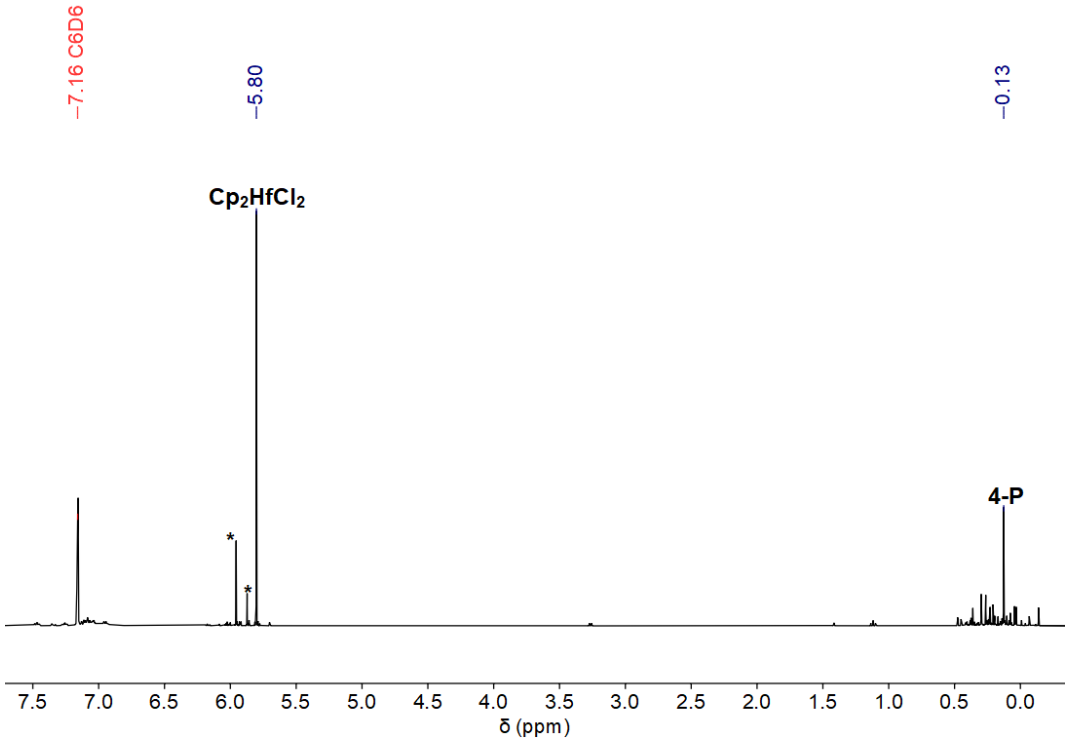

Figure S 31. ^{1}H NMR spectrum of a derivatization experiment with Ph_2PCl (25 °C, benzene-d_6, 400.13 MHz). Conditions: room temperature, benzene, 0.08 mmol Cp_2HfCl_2, 0.04 mmol $Li_2[C_3(SiMe_3)_2]$, 0.08 mmol Ph_2PCl. * denotes unknown species.

2.11.3. NMR spectra of the reaction of Cp_2HfCl_2 with $Li_2[C_3(SiMe_3)_2]$ and addition of Me_3SiI

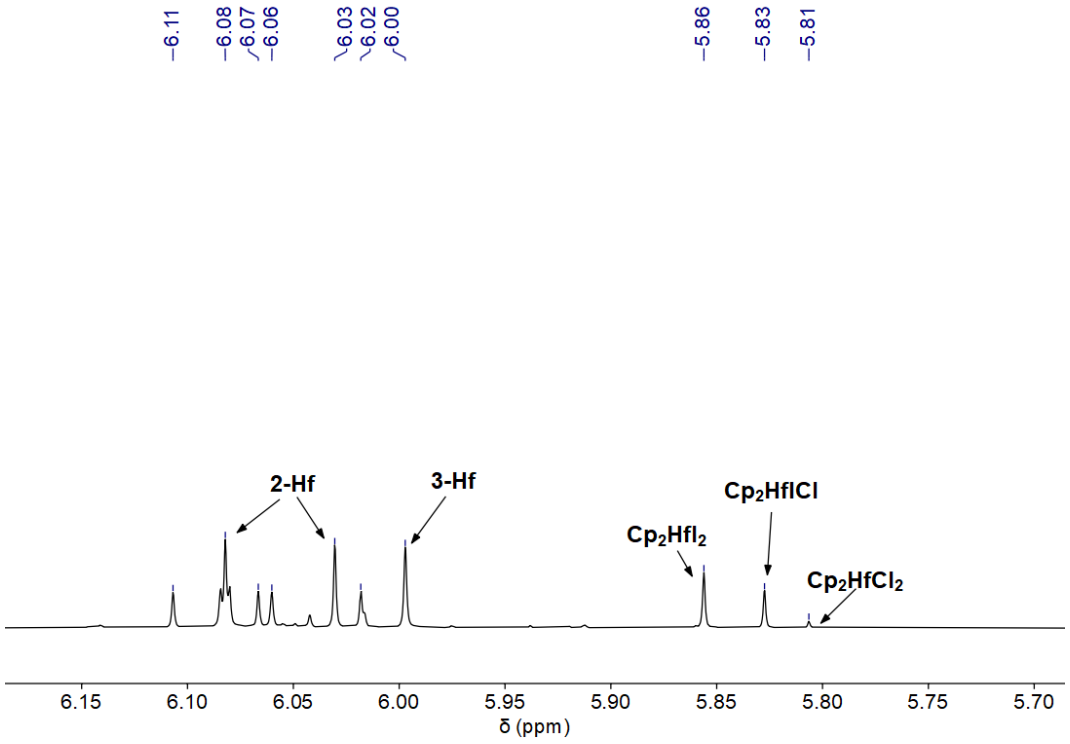

Figure S 32. ^{1}H NMR spectrum of a derivatization experiment with Me_3SiI with enlarged Cp region (25 °C, benzene-d_6, 400.13 MHz). Conditions: room temperature, benzene, 0.05 mmol Cp_2HfCl_2, 0.03 mmol $Li_2[C_3(SiMe_3)_2]$, 0.05 mmol Me_3SiI.

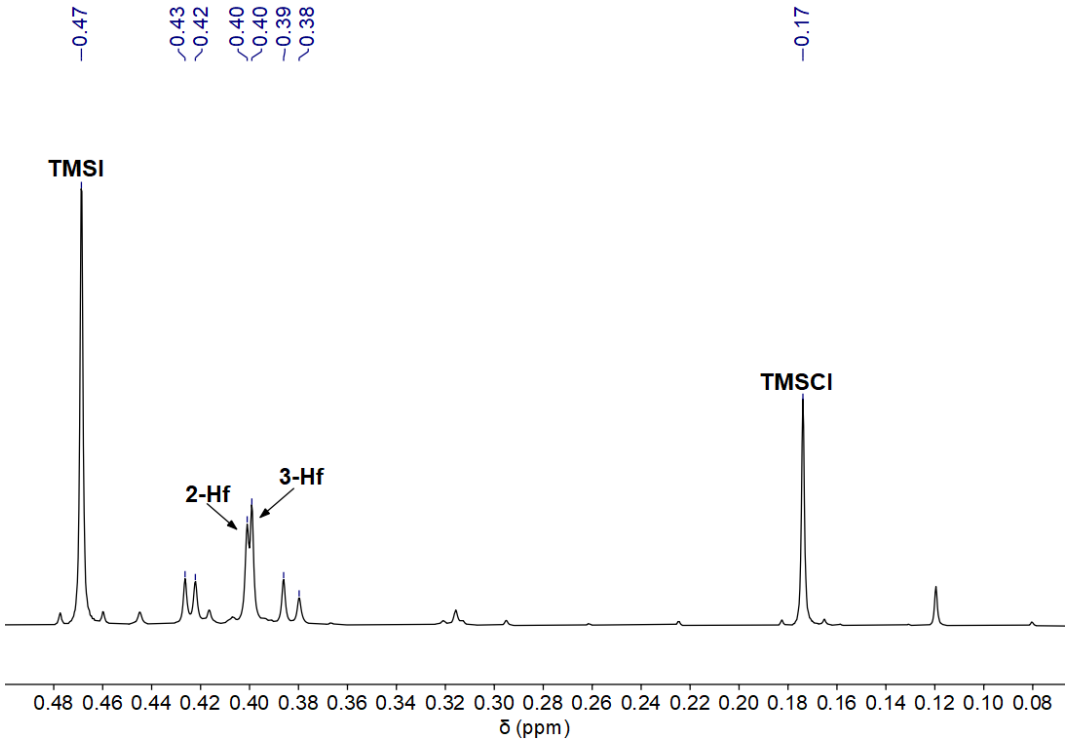

Figure S 33. ^{1}H NMR spectrum of a derivatization experiment with Me_3SiI with enlarged Me_3Si region (25 °C, benzene-d_6, 400.13 MHz). Conditions: room temperature, benzene, 0.05 mmol Cp_2HfCl_2, 0.03 mmol $Li_2[C_3(SiMe_3)_2]$, 0.05 mmol Me_3SiI.

2.11.4. NMR spectra of the reaction of Cp_2HfCl_2 with $Li_2[C_3(SiMe_3)_2]$ and addition of Me_3SiCl

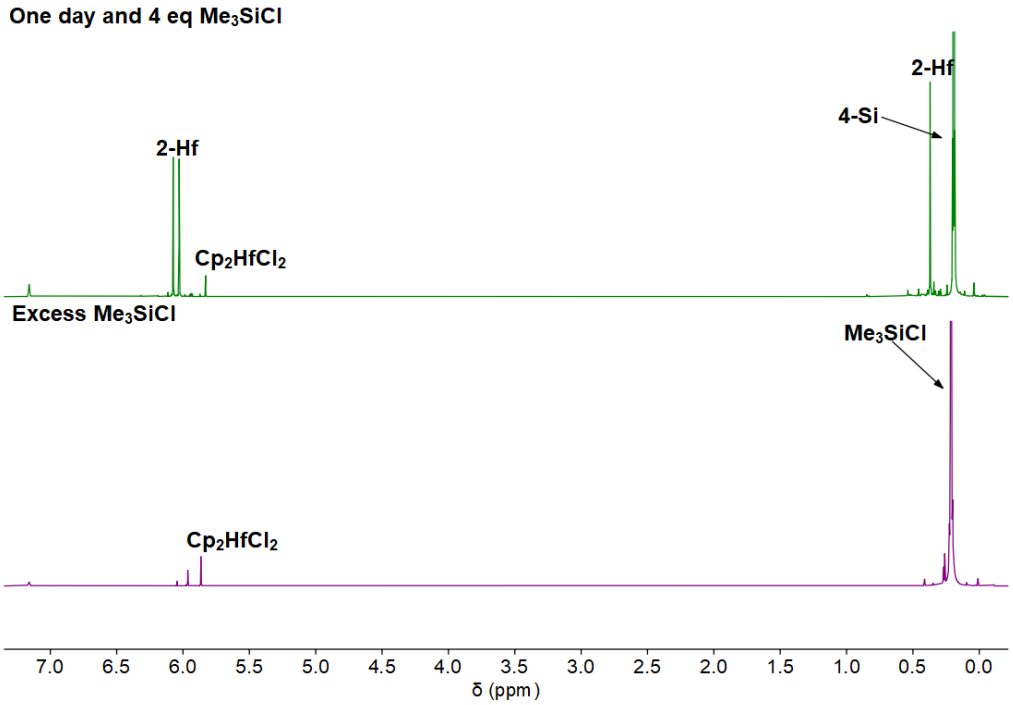

Figure S 34. Comparison of ^{1}H NMR spectra of a derivatization experiment with Me_3SiCl (25 °C, benzene-d_6, 300.20 MHz). Conditions: room temperature, benzene, 0.05 mmol Cp_2HfCl_2, 0.03 mmol $Li_2[C_3(SiMe_3)_2]$, 0.10 mmol Me_3SiCl.

3. Stability tests / Reactivity tests

3.1. Thermal stability of 2-Hf in toluene-d_8 solution

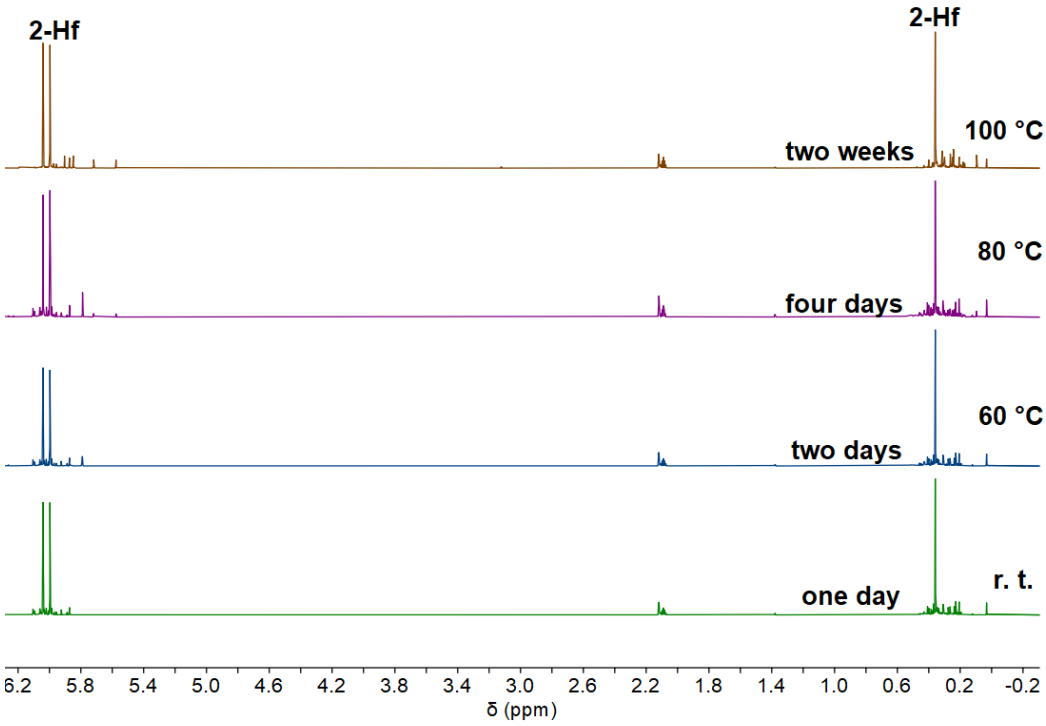

Figure S 35. Comparison of ^{1}H NMR spectra of thermal stability tests in toluene (toluene-d_8, 300.20 MHz). Conditions: room temperature, toluene, 0.80 mmol Cp_2HfCl_2, 0.40 mmol $Li_2[C_3(SiMe_3)_2]$.

3.2. Reactivity of 2-Hf with halide containing substrates

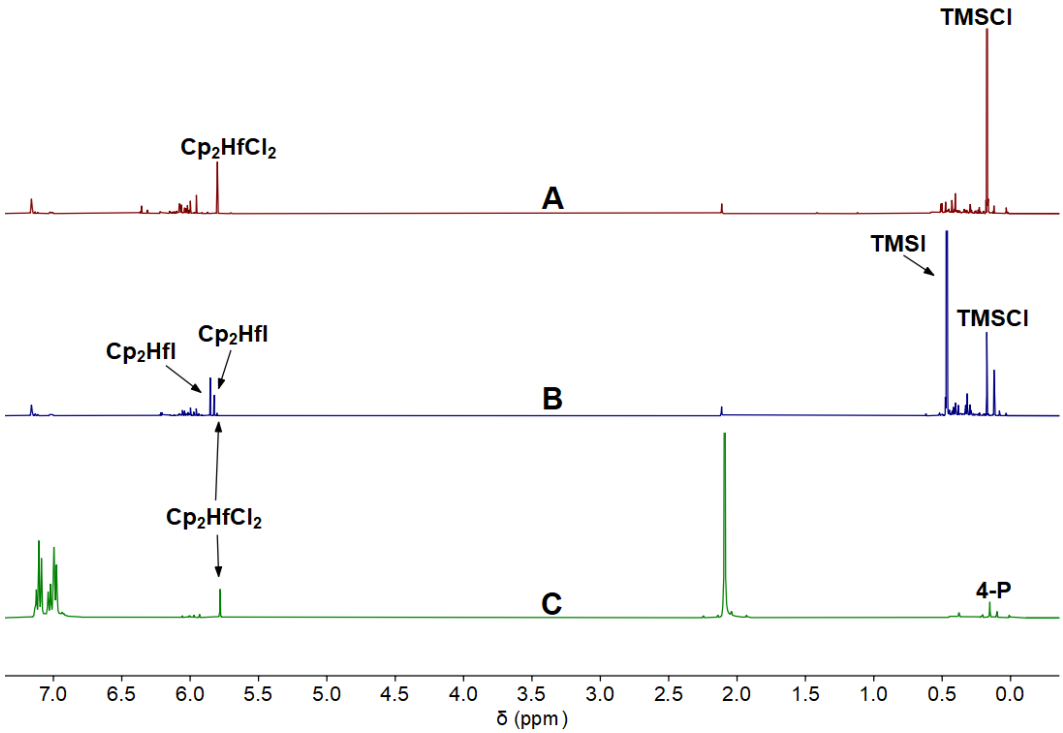

Figure S 36. Comparison of ^{1}H NMR spectra of stability tests with deferent reactants in toluene Conditions: a) 0.02 mmol **2-Hf**, 0.03 mmol TMSCl (25 °C, benzene-d_6, 400.13 MHz), b) 0.02 mmol **2-Hf**, 0.05 mmol TMSI (25 °C, benzene-d_6, 400.13 MHz), c) 0.02 mmol **2-Hf**, 0.05 mmol Ph_2PCl (25 °C, benzene-d_6, 400.13 MHz).

3.3. Reactivity tests of 2-Hf with different carbonyl compounds

3.3.1. Reactivity tests of 2-Hf with acetophenone

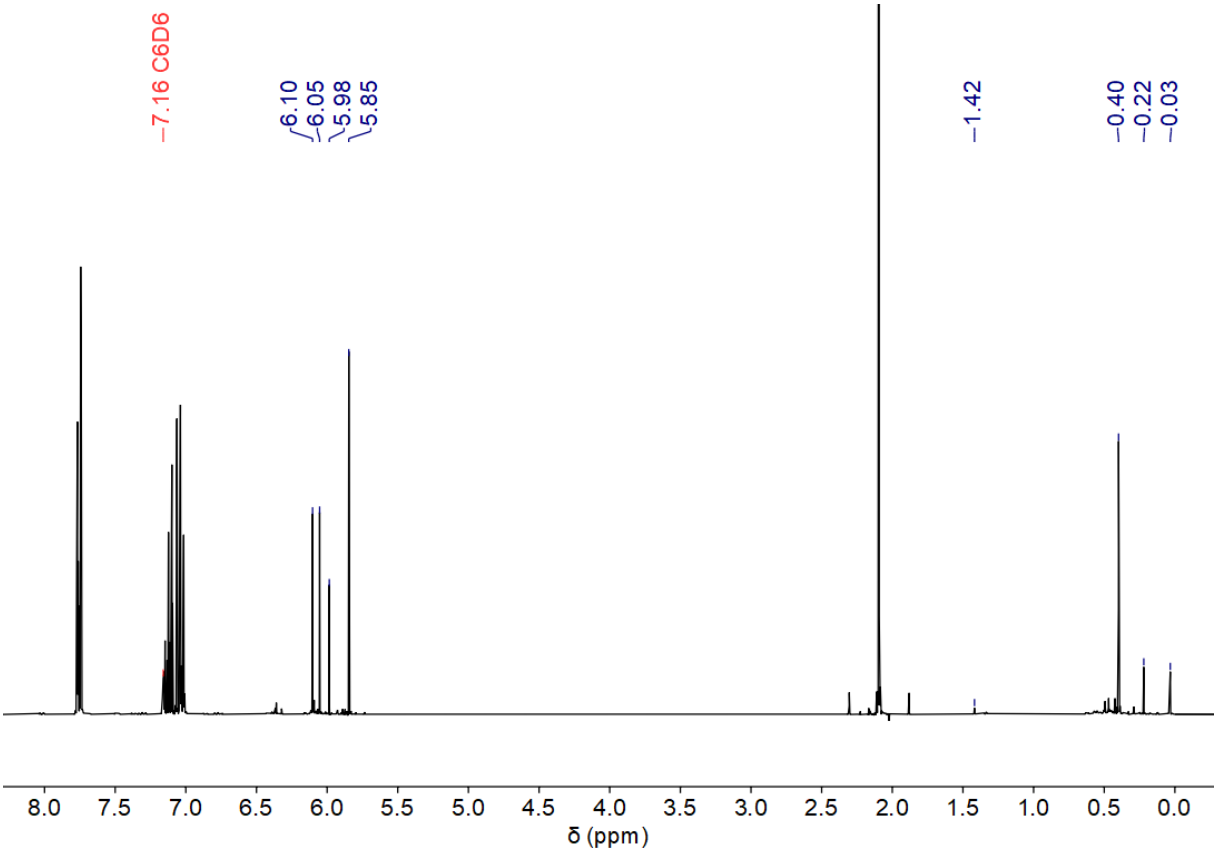

Figure S 37. ^{1}H NMR spectrum of complex **2-Hf** in presence of acetophenone, recorded after 4 hours. The spectrum shows the formation of Cp_2HfCl_2 (5.85 ppm), 1,3-bis-(trimethylsilyl)prop-1-yne (1.42, 0.22, 0.03 ppm), residual **2-Hf** (6.05, 6.10 ppm) and an unidentified new symmetrical Cp containing species (5.98 ppm). Conditions: room temperature, 0.02 mmol **2-Hf**, 0.18 mmol acetophenone (25 °C, benzene-d_6, 300.20 MHz).

3.3.2. Reactivity tests of 2-Hf with benzophenone

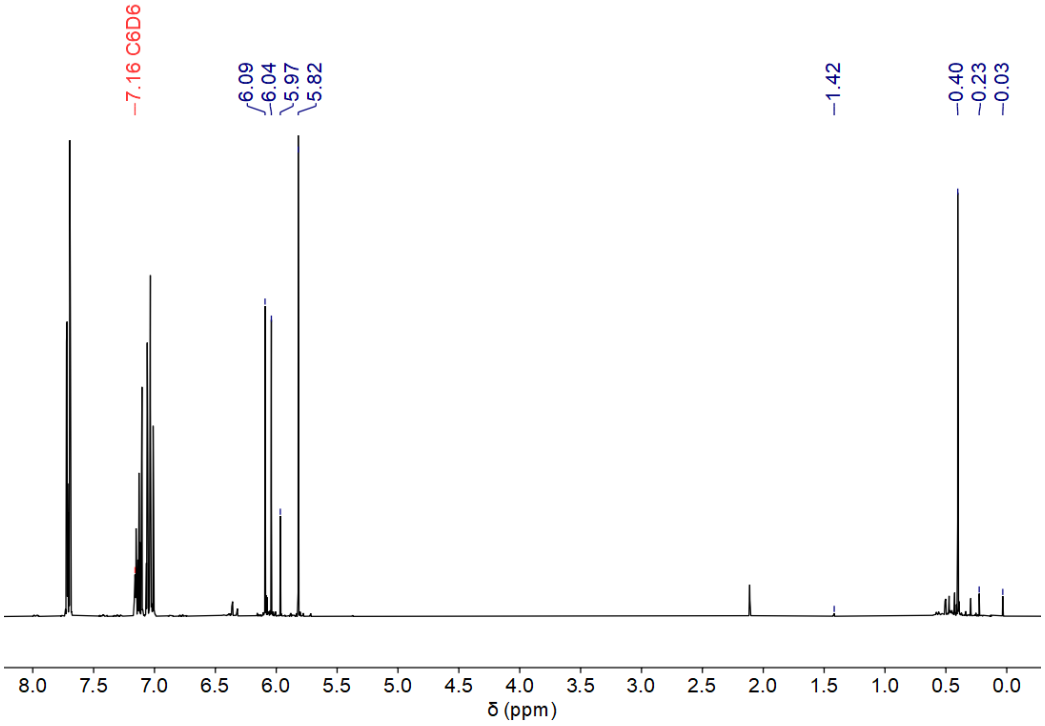

Figure S 38. ^{1}H NMR spectrum of complex **2-Hf** in presence of benzophenone, recorded after 4 hours. The spectrum shows the formation of Cp_2HfCl_2 (5.82 ppm), 1,3-bis-(trimethylsilyl)prop-1-yne (1.42, 0.22, 0.03 ppm), residual **2-Hf** (6.04, 6.09 ppm) and an unidentified new symmetrical Cp containing species (5.97 ppm). Conditions: room temperature, 0.02 mmol **2-Hf**, 0.28 mmol benzophenone (25 °C, benzene-d_6, 300.20 MHz).

3.3.3. Reactivity tests of 2-Hf with benzaldehyde

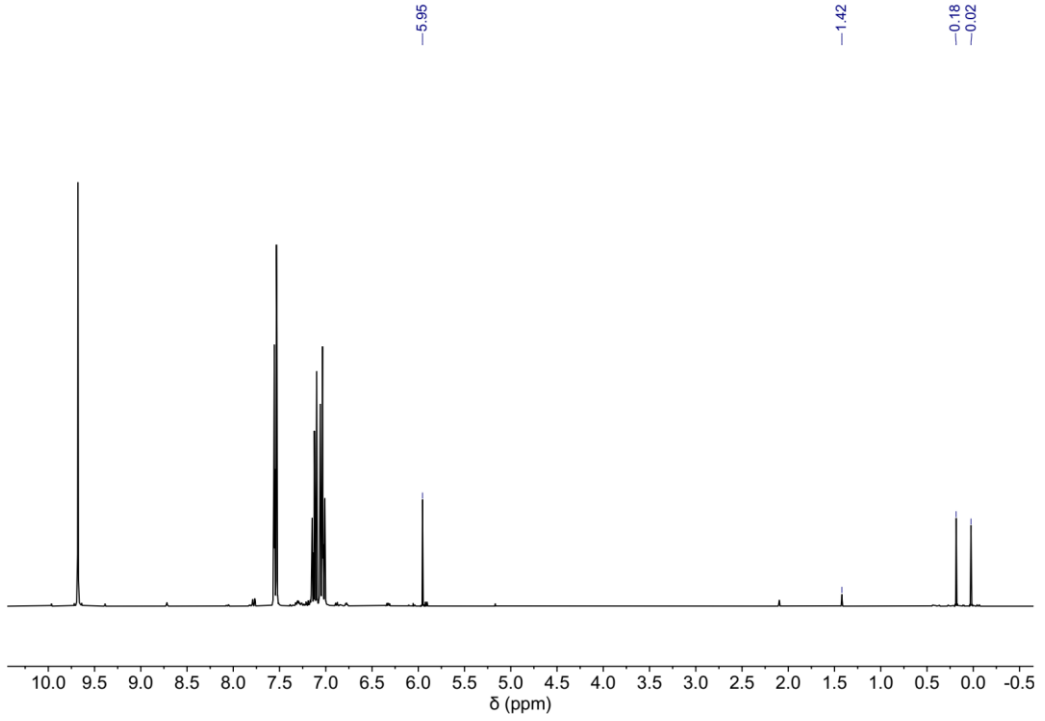

Figure S 39. ^{1}H NMR spectrum of complex **2-Hf** in presence of benzaldehyde, recorded after 4 hours. The spectrum shows the formation of *1*,3-bis-(trimethylsilyl)prop-1-yne (1.42, 0.18, 0.02 ppm) and an unidentified new symmetrical Cp containing species (5.95 ppm). Conditions: room temperature, 0.02 mmol **2-Hf**, 0.35 mmol benzaldehyde (25 °C, benzene-d_6, 300.20 MHz).

3.4. Stability tests of 3-Hf with different reactants

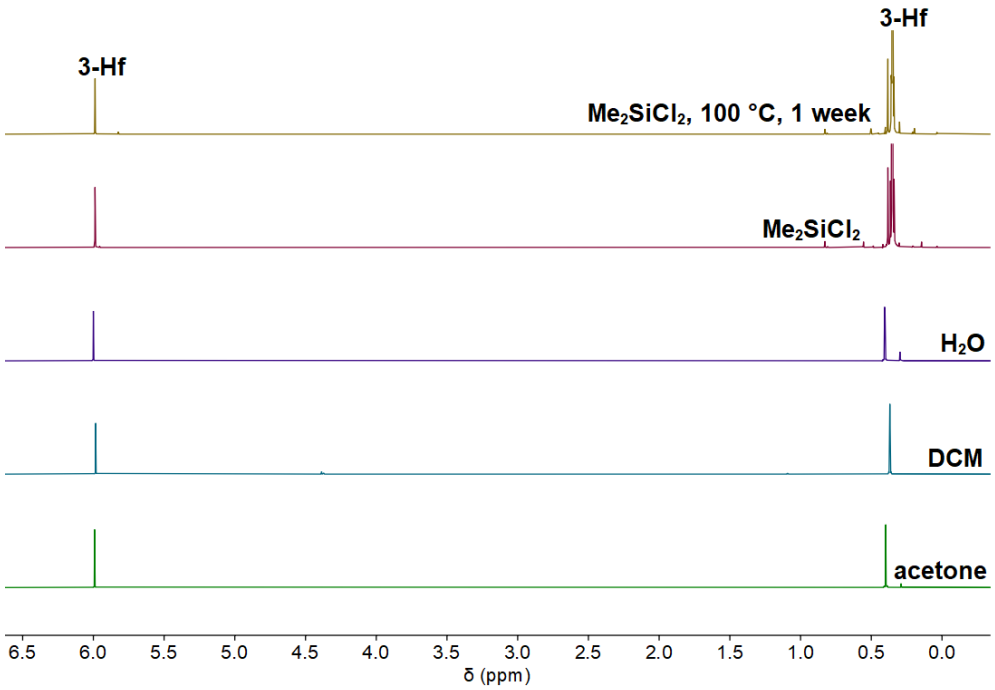

Figure S 40. Comparison of ^{1}H NMR spectra of stability tests with deferent reactants (25 °C, benzene-d_6, 300.20 MHz). Conditions: room temperature, benzene, 0.02 mmol **3-Hf**, 0.05 mL reactant.

3.5. Reactivity tests of 3-Hf with different carbonyl compounds

3.5.1. Reactivity tests of 3-Hf with acetophenone

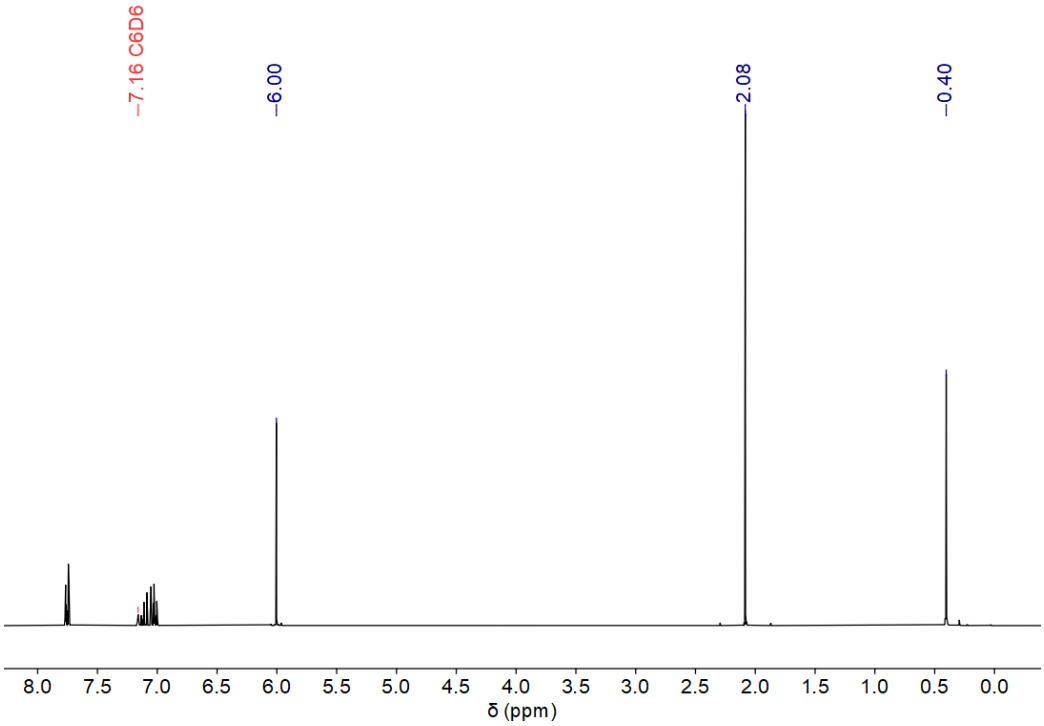

Figure S 41. ^{1}H NMR spectrum of complex **3-Hf** in presence of acetophenone. Conditions: room temperature, 0.005 mmol **3-Hf**, 0.03 mmol acetophenone (25 °C, benzene-d6, 300.20 MHz).

3.5.2. Reactivity tests of 3-Hf with benzophenone

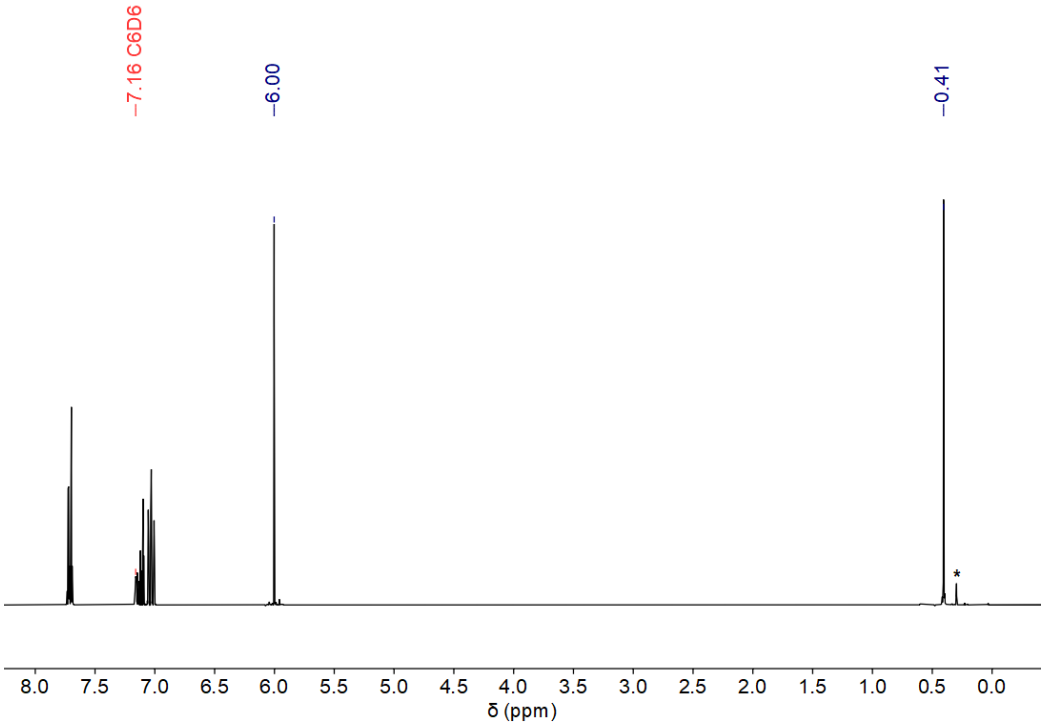

Figure S 42. ^{1}H NMR spectrum of complex **3-Hf** in presence of benzophenone. Conditions: room temperature, 0.005 mmol **3-Hf**, 0.03 mmol benzophenone (25 °C, benzene-d_6, 300.20 MHz). * indicates silicon grease.

3.5.3. Reactivity tests of 3-Hf with benzaldehyde

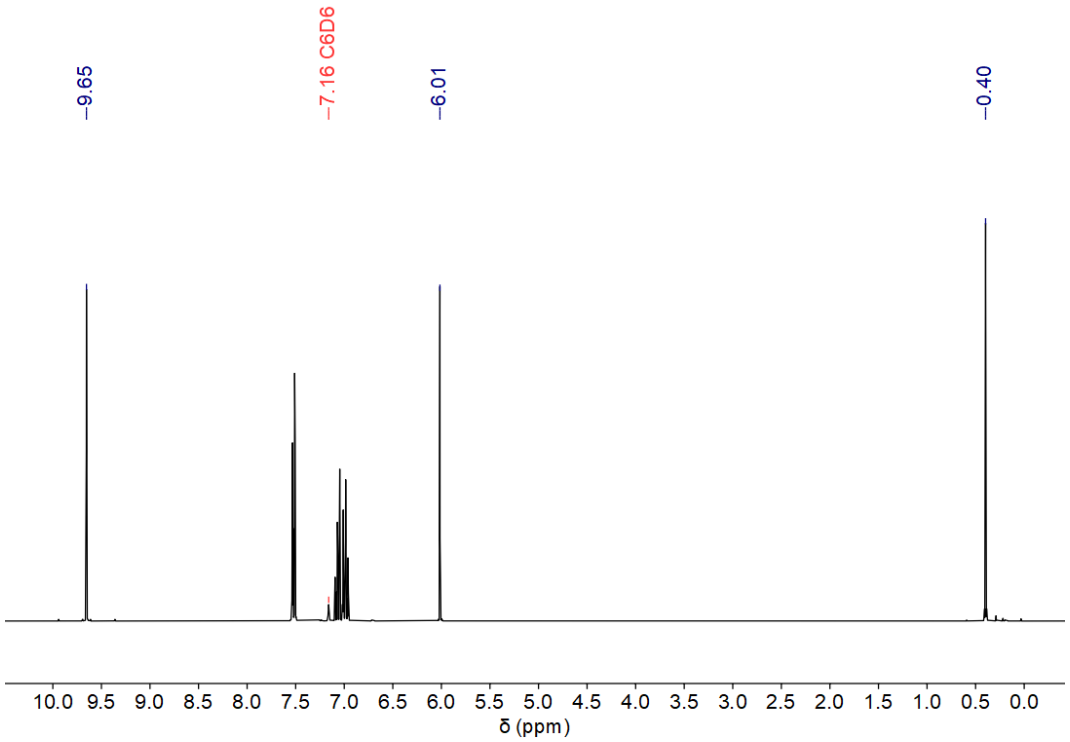

Figure S 43. ^{1}H NMR spectrum of complex **3-Hf** in presence of benzaldehyde. Conditions: room temperature, 0.007 mmol **3-Hf**, 0.04 mmol benzaldehyde (25 °C, benzene-d_6, 300.20 MHz).

3.6. Stability of complex 2-Hf in benzene

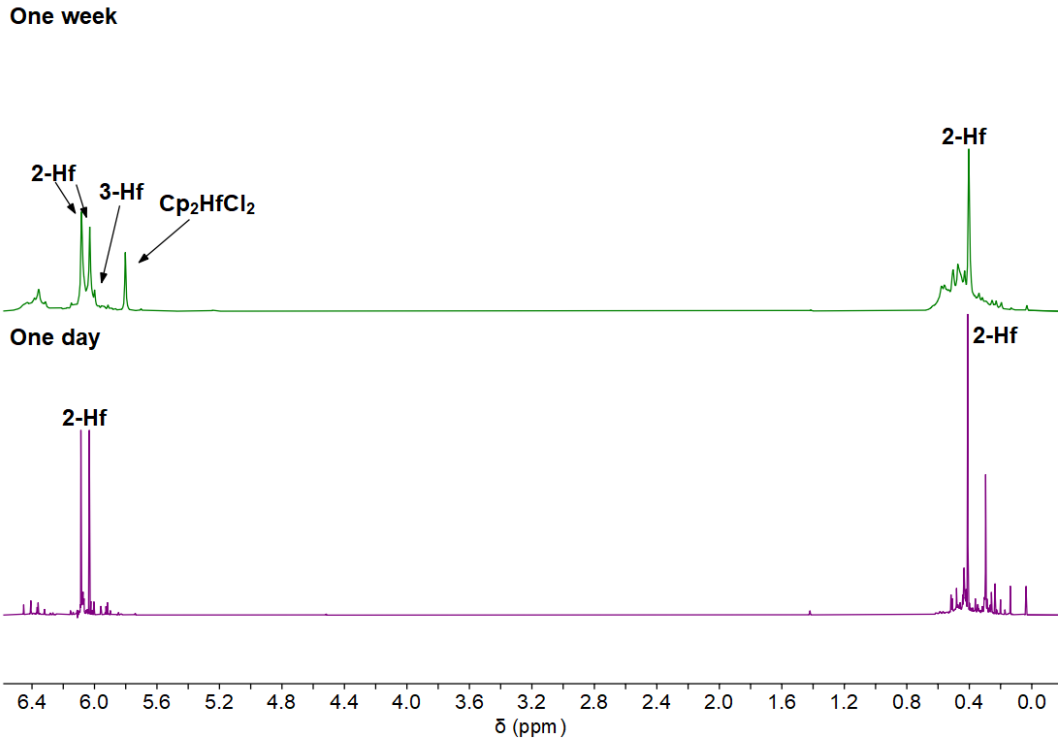

Figure S 44. Comparison of ^{1}H NMR spectrum of complex **2-Hf** in benzene (25 °C, benzene-d_6, 300.20 MHz). Conditions: room temperature, benzene, 0.05 mmol Cp_2HfCl_2, 0.03 mmol $Li_2[C_3(SiMe_3)_2]$.

3.7. Stability of complex 2-Hf in THF

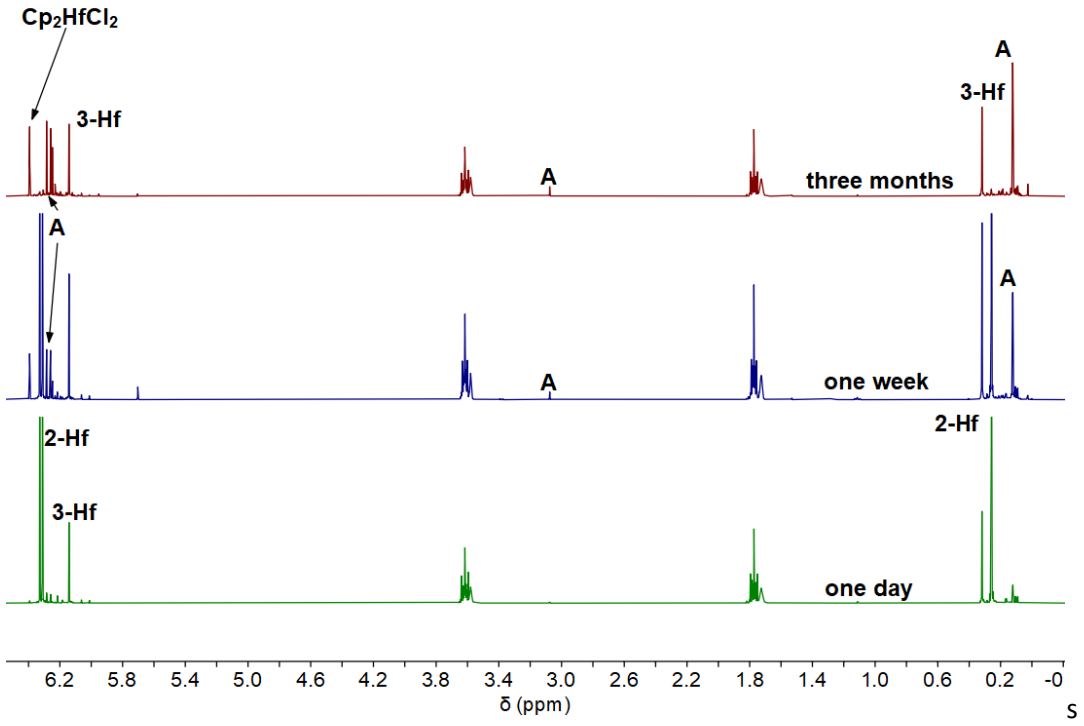

Figure S 45. Comparison of ^{1}H NMR spectra of stability tests of **2-Hf** in THF (25 °C, THF-d_8, 300.20 MHz). Conditions: room temperature, THF, 0.40 mmol Cp_2HfCl_2, 0.20 mmol $Li_2[C_3(SiMe_3)_2]$.

3.8. Stability of complex 2-Zr in benzene

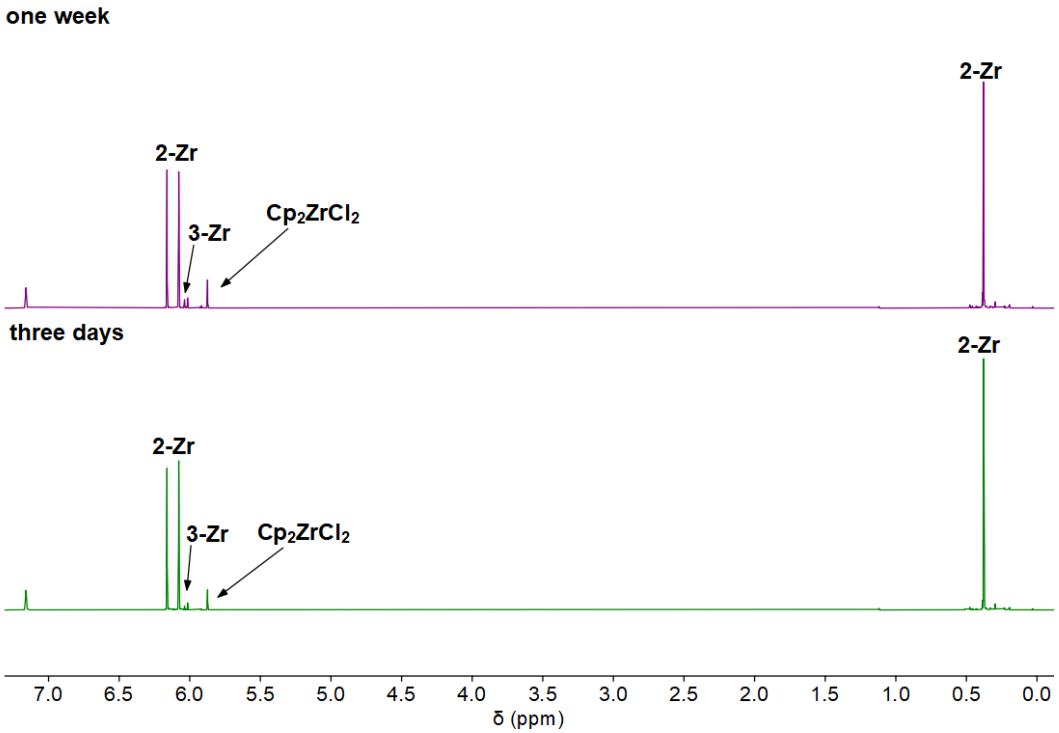

Figure S 46. ^{1}H NMR spectra of stability test of **2-Zr** in benzene (25 °C, benzene-d_6, 300.20 MHz). Conditions: room temperature, benzene, 0.02 mmol **2-Zr**.

3.9. Stability of complex 2-Zr in THF

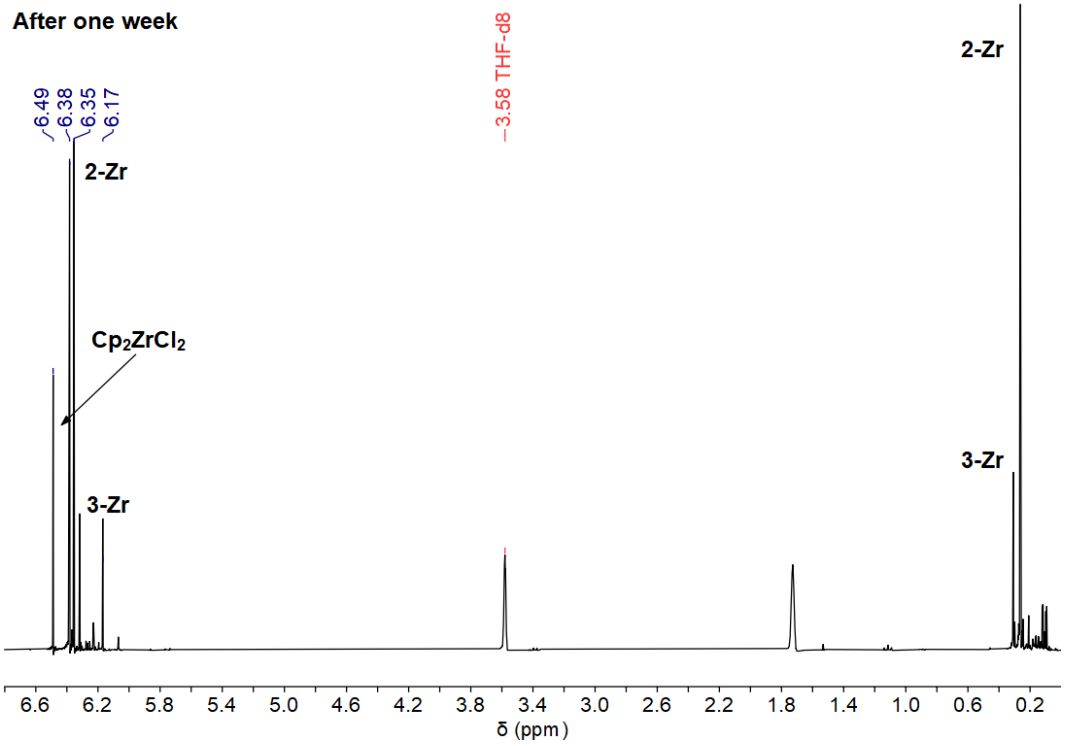

Figure S 47. ^{1}H NMR spectrum of stability test of **2-Zr** in THF (25 °C, THF-d_8, 300.20 MHz). Conditions: room temperature, THF, 0.02 mmol **2-Zr**.

3.10. Stability of complex 2-Hf in the presence of LiCl

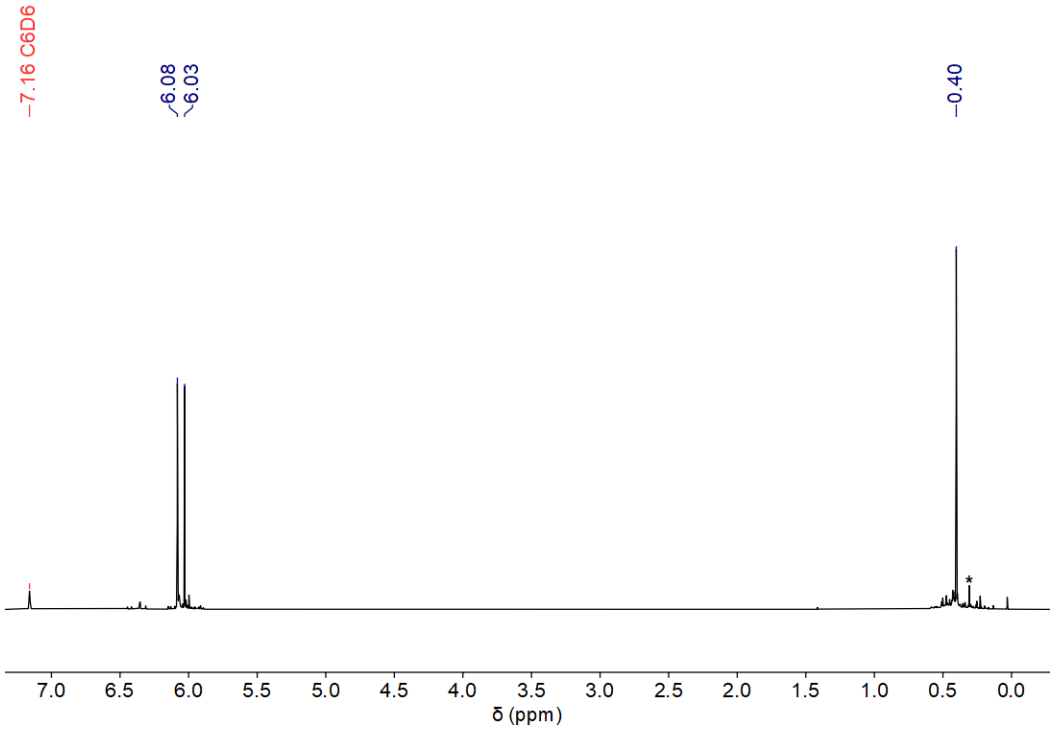

Figure S 48. ^{1}H NMR spectrum of complex **2-Hf** in presence of LiCl. Conditions: room temperature, 0.02 mmol **2-Hf**, 0.50 mmol LiCl (25 °C, benzene-d_6, 400.13 MHz). * indicates silicon grease.

3.11. Stability of complex 3-Hf in the presence of LiCl

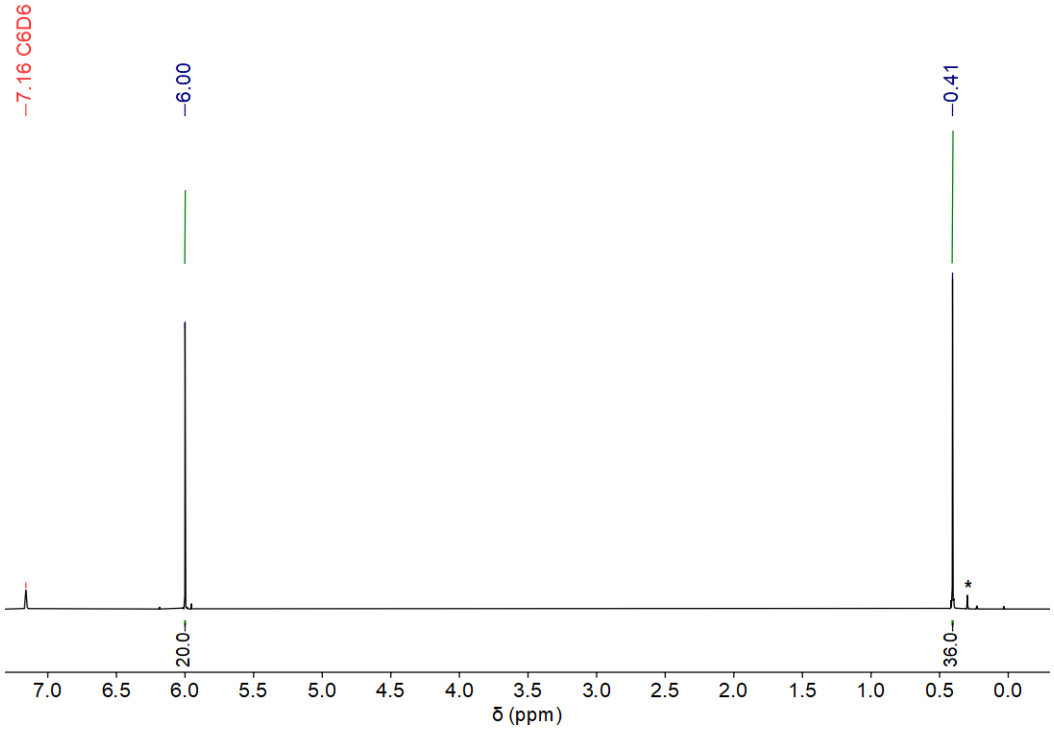

Figure S 49. ^{1}H NMR spectrum of complex **3-Hf** in presence of LiCl. Conditions: room temperature, 0.005 mmol **3-Hf**, 0.50 mmol LiCl (25 °C, benzene-d_6, 400.13 MHz). * indicates silicon grease.

4. Crystallographic details

Table S 1. Crystallographic details of **2-Hf**, **3-Hf** and **4-P.**

	2-Hf	**3-Hf**	**4-P**	**Cp_2HfI_2**
Chem. Formula	$C_{29}H_{38}Cl_2Hf_2Si_2$	$C_{38}H_{56}Hf_2Si_4$	$C_{36}H_{41}P_2Si_2$	$C_{10}H_{10}HfI_2$
Form. Wght [g mol^{-1}]	870.65	982.16	591.81	562.47
Colour	yellow	red	colourless	colourless
Cryst. system	monoclinic	tetragonal	orthorhombic	monoclinic
Space group	*Cc*	$P4_2bc$	*Iba*2	*C*2/*c*
a [Å]	33.568(3)	25.1478(6)	17.3177(3)	13.8133(8)
b [Å]	11.9648(11)	25.1478(6)	33.3177(7)	7.2670(4)
c [Å]	16.4050(15)	12.3953(3)	12.0156(2)	13.2925(11)
α [°]	90	90	90	90
β [°]	110.6513(16)	90	90	115.9730(8)
γ [°]	90	90	90	90
V [$Å^3$]	6165.5(10)	7838.9(4)	6932.8(2)	1199.55(14)
Z	8	8	8	4
$\rho_{calc.}$ [g cm^{-3}]	1.876	1.664	1.134	3.115
μ [mm^{-1}]	6.998	5.441	1.957	13.799
T [K]	150(2)	150(2)	150(2)	150(2)
radiation type	Mo Kα	Mo Kα	Cu Kα	Mo Kα
reflections measured	50870	107575	38417	16486
independent reflections	13887	9464	5758	1623
observed reflections with $I > 2\sigma(I)$	13316	9071	5616	1561
$R_{int.}$	0.0290	0.0336	0.0403	0.0292
F(000)	3344	3872	2520	992
R_1 ($I > 2\sigma(I)$)	0.0241	0.0225	0.0271	0.0152
wR_2 (all data)	0.0567	0.0566	0.0706	0.0353
GOF on F^2	1.040	1.014	1.029	1.118
Parameters	672	409	395	60
CCDC number	2092157	2092158	2092159	2092160

Table S 2. Comparison of structural parameters of **2-Zr**, **3-Zr**, **2-Hf** and **3-Hf**. M = Zr, Hf, values in italics are taken from optimized structures on the level of theory B3LYP/GD3BJ/def2tzvp**,** [a] in the optimized structure both bonds are identical.

	2-Zr$_{in\text{-}in}$	2-Zr$_{in\text{-}out}$	2-Hf$_{in\text{-}in}$	2-Hf$_{in\text{-}out}$	3-Zr	3-Hf
M-C [Å]	2.282(4)	2.265(4)$_{in}$	2.252(7)	2.251(7)$_{out}$	2.283(3)	2.248(5)
	2.288(4)	2.272(4)$_{out}$	2.239(6)	2.268(6)$_{in}$	2.295(3),	2.269(5)
	2.259[a]	*2.258*$_{in}$	*2.249*[a]	*2.251*$_{in}$	2.306(3)	2.259(5)
		2.267$_{out}$		*2.258*$_{out}$	2.287(3)	2.258(5)
					2.288	*2.277*
					2.272[a]	*2.261*[a]
M-Cl [Å]	2.4437(13)	2.445(1)$_{in}$	2.413(2)	2.422(2)$_{out}$	-	-
	2.4432(11)	2.456(1)$_{out}$	2.428(2)	2.414(2)$_{in}$		
	2.455[a]	*2.439*$_{in}$	*2.441*[a]	*2.427*$_{in}$		
		2.439$_{out}$		*2.431*$_{out}$		
C_1=C_2, C_2=C_3 [Å]	1.306(6)	1.319(6)	1.298(9)	1.314(9)	1.313(4)	1.307(7)
	1.310(6)	1.303(6)	1.317(9)	1.317(9)	1.310(4)	1.330(7)
	1.305[a]	*1.310*$_{in}$	*1.306*[a]	*1.311*$_{in}$	*1.302*	*1.303*
		1.302$_{out}$		*1.302*$_{out}$	*1.306*	*1.307*
C_4=C_5, C_5=C_6 [Å]	-	-	-	-	1.309(4)	1.306(7)
					1.306(4)	1.312(7)
IR: C=C=C [cm^{-1}]	1776	1776	1844	1844	1772	1793
	1882	*1878*	*1887*	*1882*	1784	1775
					1862$_{out\text{-}ph.}$	*1863*$_{out\text{-}ph.}$
					1887$_{in\text{-}ph.}$	*1891*$_{in\text{-}ph.}$
δ ^{13}C *C*=C=*C* [ppm]	106.5	106.5	101.6	101.6	105.4	106.1
δ ^{13}C C=*C*=C [ppm]	174.7	174.7	182.8	182.8	171.4	177.8

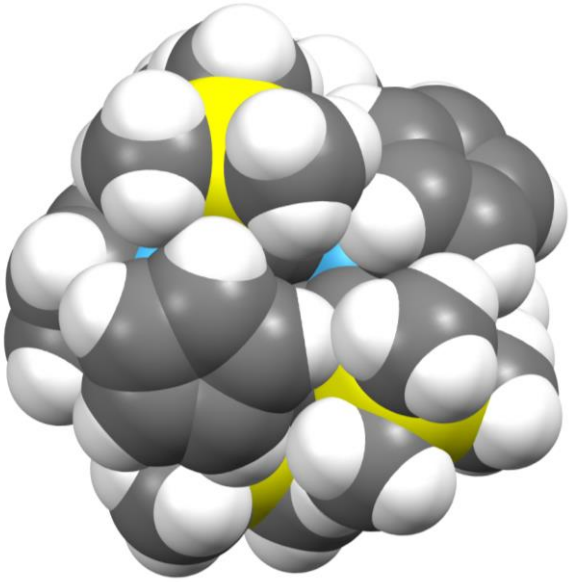

Figure S 50. Space-filling model of complex **3-Hf**.

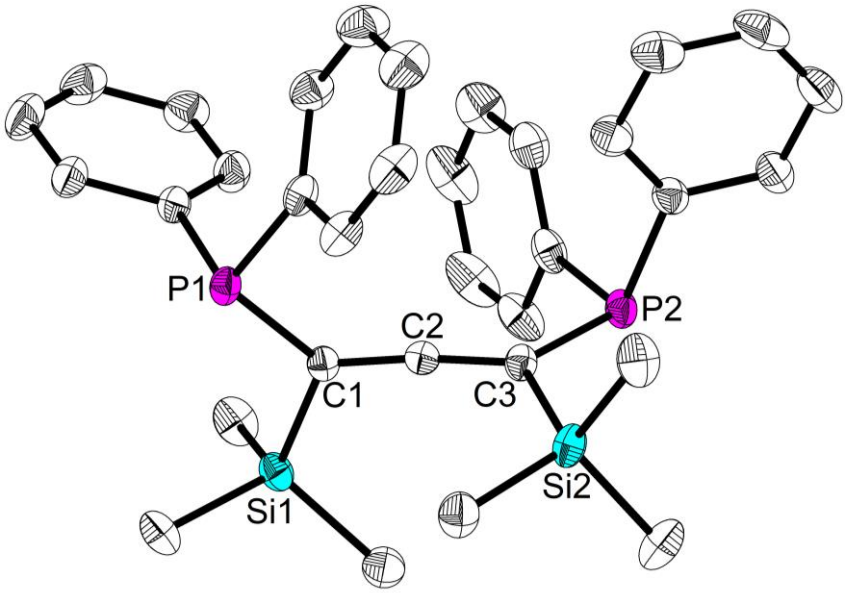

Figure S 51. Molecular structure of complex **4-P**. Thermal ellipsoids correspond to 30% probability. Hydrogen atoms as well as disordered solvent molecule (benzene) are omitted for clarity.

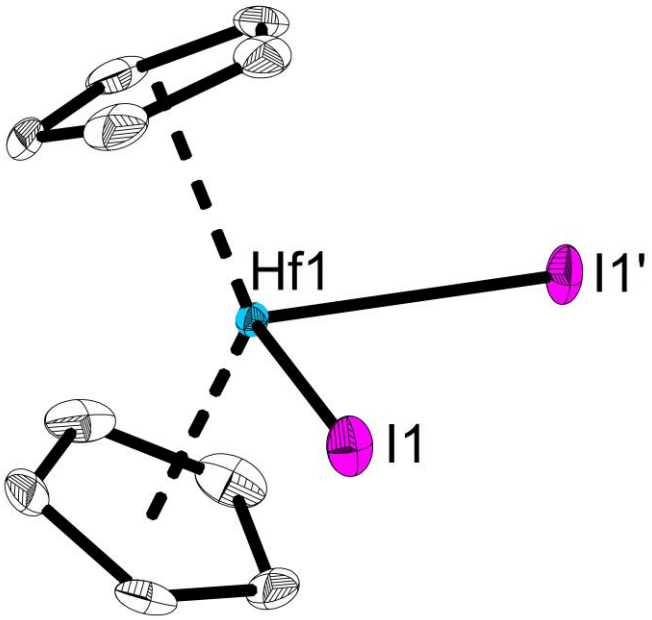

Figure S 52. Molecular structure of **Cp_2HfI_2**. Thermal ellipsoids correspond to 30% probability. Hydrogen atoms are omitted for clarity.

5. Details of vibrational spectroscopy

In this chapter the experimental IR and Raman spectra are presented.

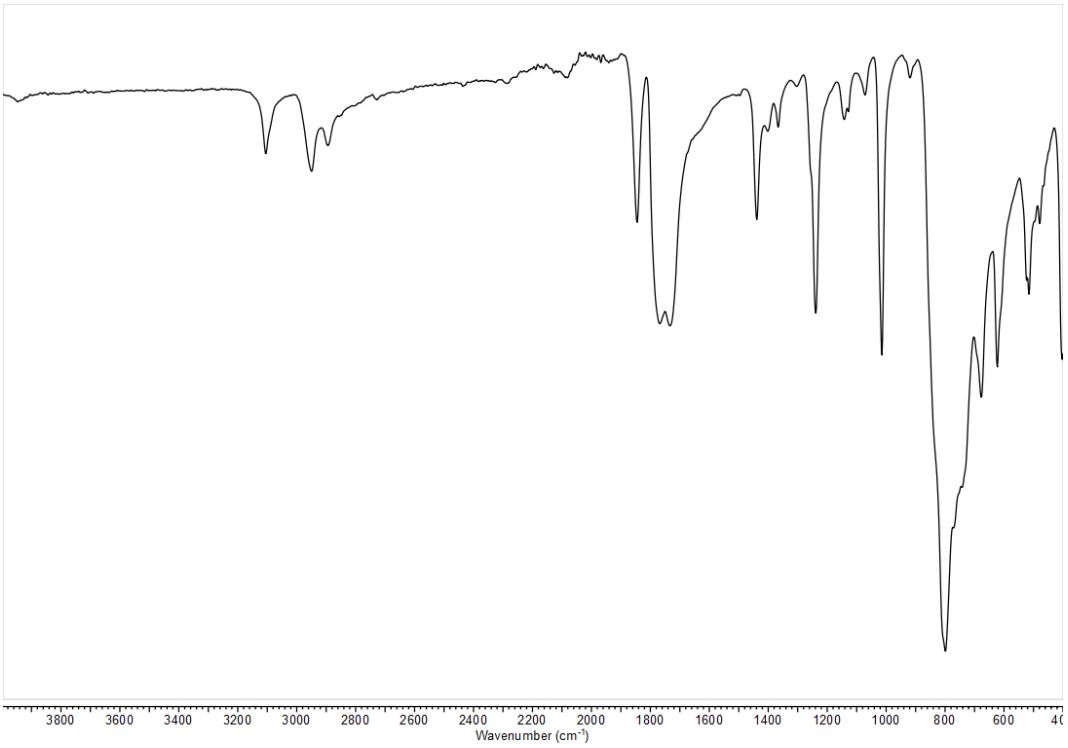

Figure S 53. IR spectrum of **2-Hf**.

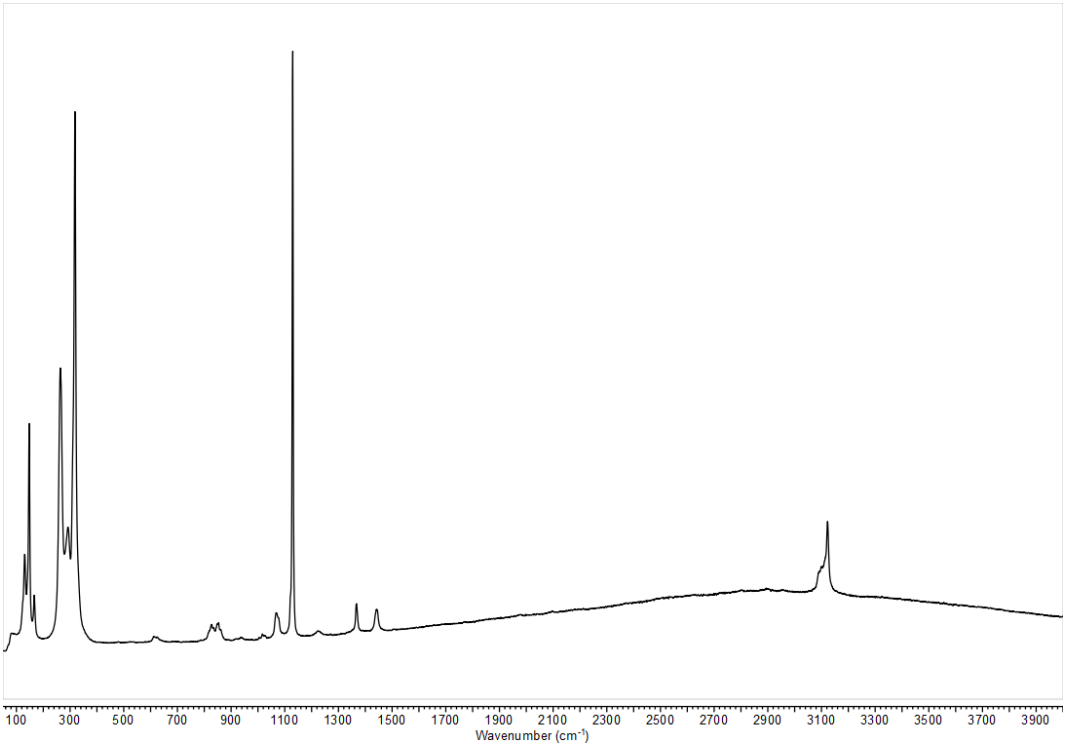

Figure S 54. Raman spectrum of complex **2-Hf**.

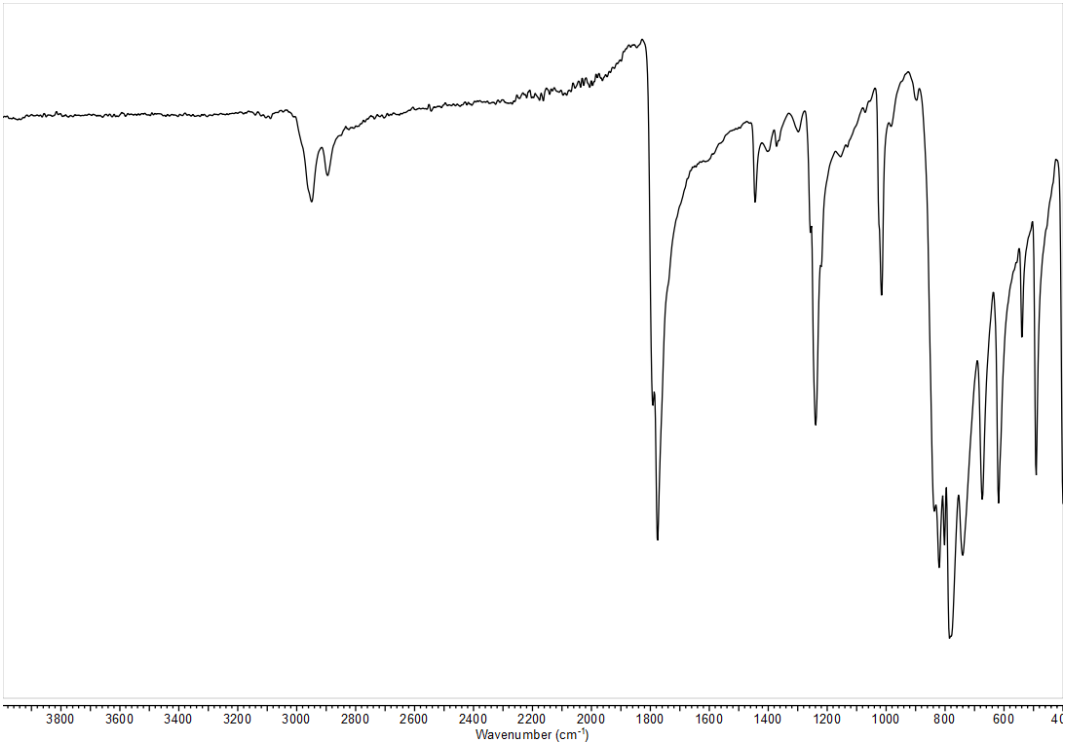

Figure S 55. IR spectrum of complex **3-Hf**.

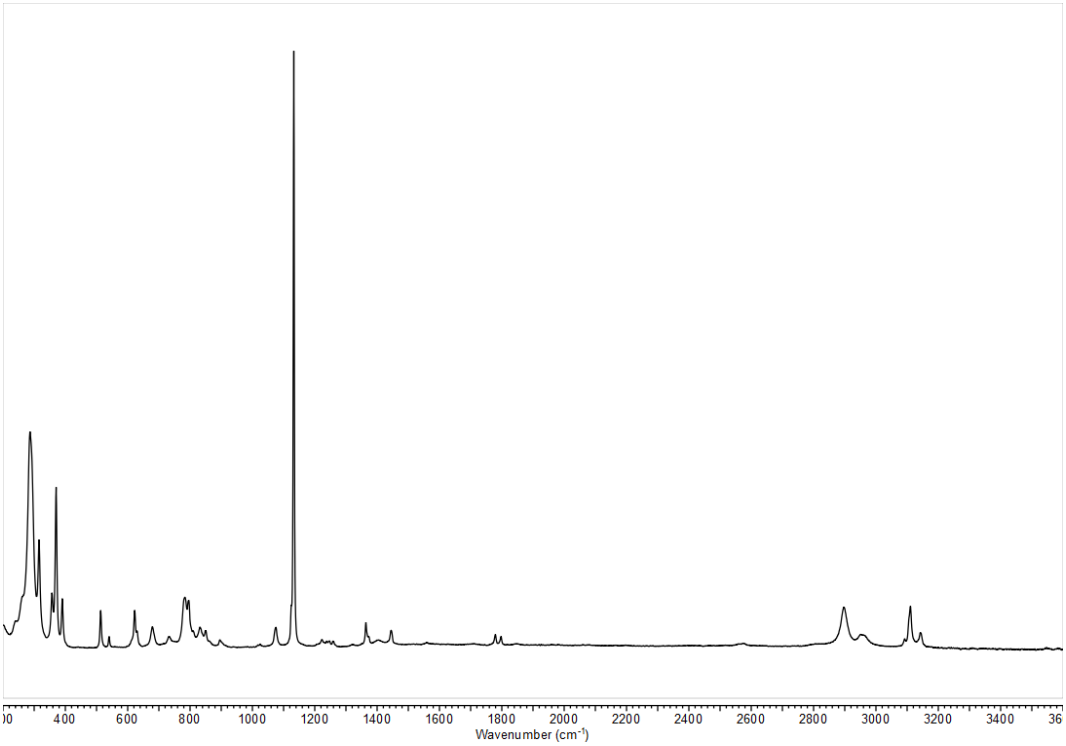

Figure S 56. RAMAN spectrum of **3-Hf**.

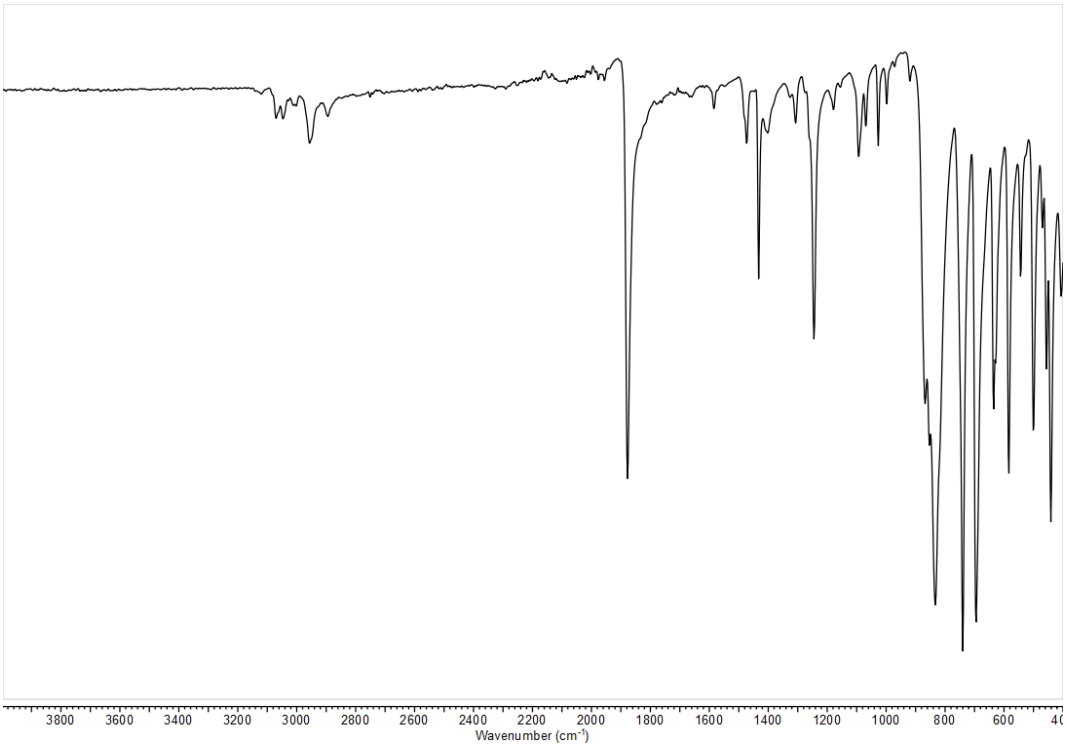

Figure S 57. IR spectrum of **4-P**.

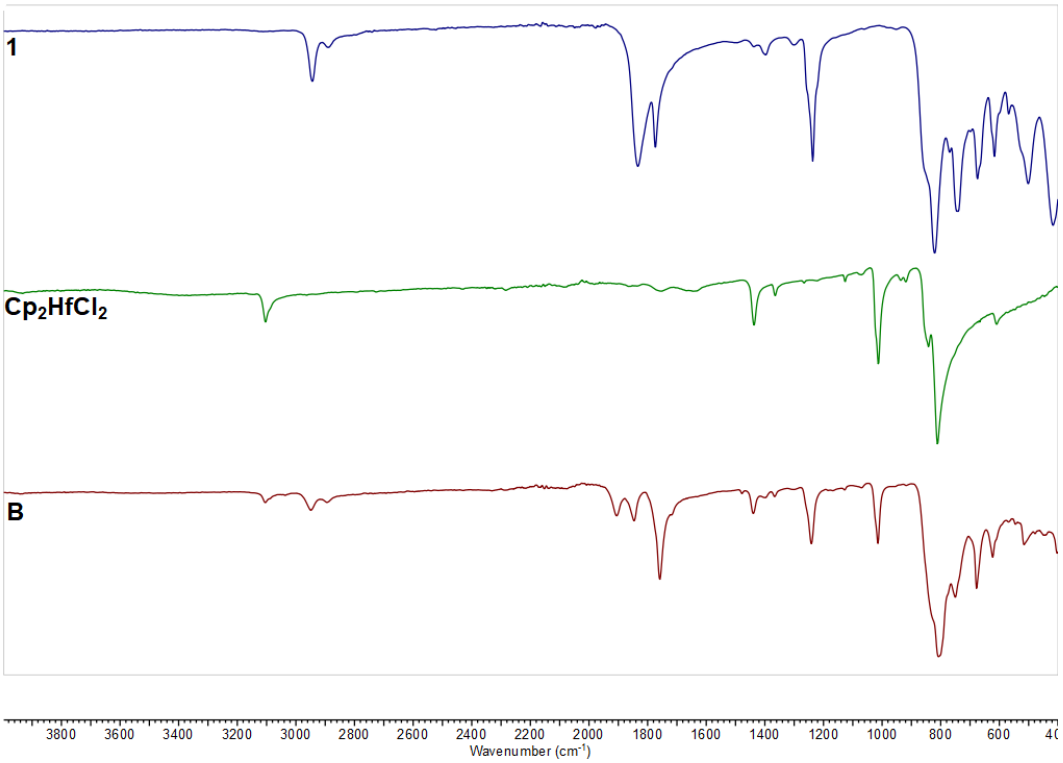

Figure S 58. Comparison of IR spectra of **1**, Cp_2HfCl_2 and **B**.

6. Computational details

6.1. General Remarks

Computations were carried out using *Gaussian16.*[9] We investigated the thermodynamic feasibility of the reaction between Cp_2HfCl_2 and the dilithioallene precursor **1**. To avoid the quantuum theoretical problem of LiCl formation we used an isodesmic exchange reaction, developed earlier.[10] For these investigations we considered the complexes Cp'_2MMe_2 that react with methyl allenes with formation of ethane and the metallocene complex of interest (e.g. Scheme S 1). Therefore, we optimized the real-size molecules using the hybrid density functional method B3LYP,[11,12] in combination with the basis set def2tzvp,[13] and the empirical dispersion correction GD3BJ[14] (notation: B3LYP/GD3BJ/def2tzvp). Vibrational frequencies were also computed, to include zero-point vibrational energies in thermodynamic parameters and to characterize all structures as minima on the potential energy surface. In addition to the electronic supporting information, we provide a multi-structure xyz-file including all calculated molecules.

Please note that all computations were carried out for single, isolated molecules in the gas phase (ideal gas approximation). There may well be significant differences between gas phase and condensed phase.

6.2. Thermochemisty

In this chapter we summarize the results of our thermodynamic calculations, which were performed on the B3LYP/GD3BJ/def2stzvp level of theory as described above. At first, we optimized the molecular structures of three different $[(Cp_2MCl)_2(C_3(SiMe_3)_2]$ (**2-M**) (M = Ti, Zr, Hf) isomers. Regarding the position of the Cl atom with respect to the allene unit, we considered the **2-M**$_{out\text{-}out}$, **2-M**$_{in\text{-}out}$ and **2-M**$_{in\text{-}in}$ complexes. Based on the Gibbs free reaction energies the latter turned out to be the thermodynamically preferred isomer for all **2-M** systems, even if all species are nearly thermoneutral to each other (Table S 3). It should be noted that **2-Ti** is so far only hypothetical and all attempts to synthesize it have failed until now.[15]

Table S 3: Comparison of the reaction enthalpies and energies referring to the 2-M$_{in\text{-}in}$ isomers.

Isomer referred to 2-M$_{in\text{-}in}$	Δ_RH [kJ/mol]	Δ_RG [kJ/mol]	Δ_RH [kcal/mol]	Δ_RG [kcal/mol]
2-Ti$_{in\text{-}out}$	11.3	2.7	2.7	2.7
2-Ti$_{out\text{-}out}$	18.2	5.3	4.3	5.3
2-Zr$_{in\text{-}out}$	13.4	12.5	3.2	3.0
2-Zr$_{out\text{-}out}$	15.2	22.2	3.6	5.3
2-Hf$_{in\text{-}out}$	10.3	8.4	2.5	2.0
2-Hf$_{out\text{-}out}$	11.3	17.2	2.7	4.1

These results explain the presence of both isomers (**2-M**$_{in\text{-}out}$ and **2-M**$_{in\text{-}in}$) in the molecular structure determined by SC-XRD. In the following we referred our calculations to the **2-M**$_{in\text{-}in}$ isomers. To explain the different reactivity of the group 4 complexes we had a closer look at the Gibbs free energies of the formation of hypothetical metallacyclobutadiene complexes **MA** and compared these with Gibbs free energy values for the obtained complexes **2-M** and **3-M** (only M = Zr and Hf known) (see Scheme S 1 - Scheme S 3; Table S 4 - Table S 6).

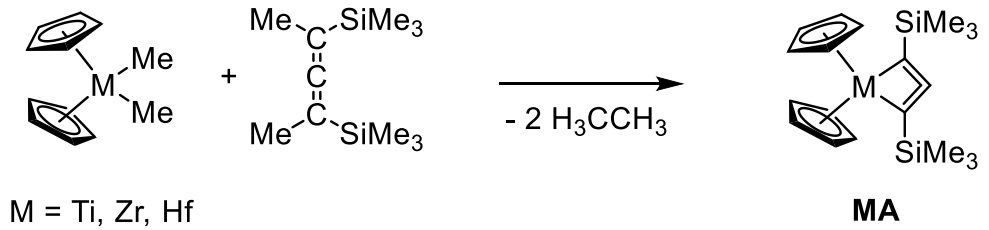

Scheme S 1: Investigated isodesmic exchange reaction to give metallacyclobutadiene complexes **MA**.

Table S 4: Reaction enthalpies and energies for the formation of **MA** complexes.

Product	Δ_RH [kJ/mol]	Δ_RG [kJ/mol]	Δ_RH [kcal/mol]	Δ_RG [kcal/mol]
TiA	-2.41	-26.43	-0.58	-6.32
ZrA	1.32	-18.30	0.32	-4.37
HfA	21.05	2.63	5.03	0.63

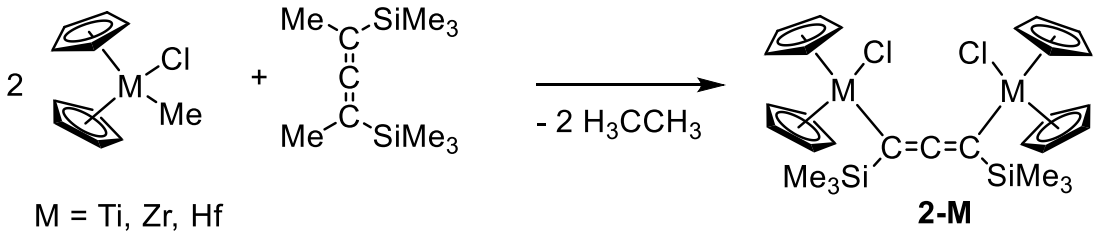

Scheme S 2: Investigated isodesmic exchange reaction to give complexes **2-M**.

Table S 5. Reaction enthalpies and energies for the formation of **2-M** complexes.

Product	Δ_RH [kJ/mol]	Δ_RG [kJ/mol]	Δ_RH [kcal/mol]	Δ_RG [kcal/mol]
2-Ti$_{inin}$	-115.48	-72.78	-27.60	-17.39
2-Zr$_{inin}$	-146.04	-103.40	-34.90	-24.71
2-Hf$_{inin}$	-139.92	-96.50	-33.44	-23.06

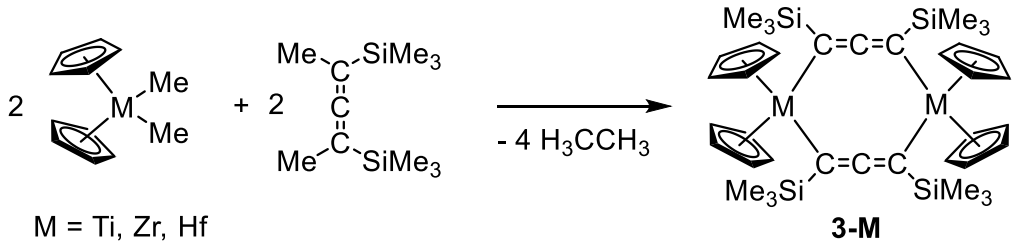

Scheme S 3: Investigated isodesmic exchange reaction to give complexes **3-M**.

Table S 6: Reaction enthalpies and energies for the formation of **3-M** complexes.

Product	Δ_RH [kJ/mol]	Δ_RG [kJ/mol]	Δ_RH [kcal/mol]	Δ_RG [kcal/mol]
3-Ti	-196.5	-153.1	-47.0	-36.6
3-Zr	-256.7	-216.8	-61.4	-51.8
3-Hf	-243.6	-200.6	-58.2	-48.0

These data clearly reveal the preferred formation of the complexes **2-M** and **3-M** compared to the **MA** complexes which is well in line with the observed reactivity. Furthermore, we were interested in the rearrangement reactions of **2-M** complexes which takes place in polar solvents and leads to **3-M** and Cp_2MCl_2 (M = Zr, Hf). Therefore, we again calculated the Gibbs free energies and reaction enthalpies and observed endothermic values for these reactions (B3LYP/GD3BJ/def2stzvp, Scheme S 4 and Table S 7). Since this reaction shows a strong solvent dependence, we next performed solvent corrected smd[16] calculations as single point calculation using the optimized structures (Scheme S 4 and Table S 7, all attempts to optimize the structures of **3-M** complexes with smd failed).

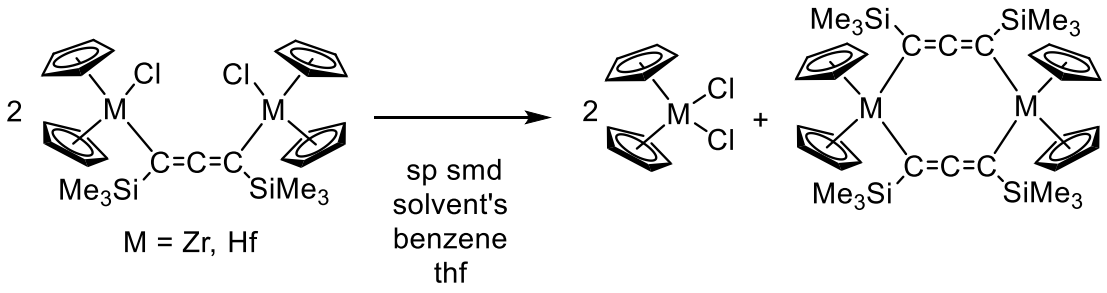

Scheme S 4: Investigated isodesmic exchange reaction of **2-M** to give complexes **3-M** and Cp_2MCl_2.

The solvent corrected energies are in all cases exergonic but endothermic. The values for reactions in benzene are slightly more endothermic, which could serve as an explanation for the observed reactivity.

Table S 7: Reaction enthalpies and energies for the formation of **3-M** and Cp_2MCl_2 from **2-M** complexes.

Starting material	Δ_RH [kJ/mol]	Δ_RG [kJ/mol]	Δ_RH [kcal/mol]	Δ_RG [kcal/mol]
2-Zr	68.3	17.8	16.3	4.3
2-Hf	63.8	11.5	15.3	2.8
2-Zr sp smd benzene	61.4	-44.3	14.7	-10.6
2-Hf sp smd benzene	63.7	-27.3	15.2	-6.5
2-Zr sp smd thf	45.8	-36.5	10.9	-8.7
2-Hf sp smd thf	42.4	-45.9	10.1	-11.0

7. References

[1] Reiß, F.; Reiß, M.; Spannenberg, A.; Jiao, H.; Baumann, W.; Arndt, P.; Rosenthal, U.; Beweries, T., Visiting the Limits between a Highly Strained 1-Zirconacyclobuta-2,3-diene and Chemically Robust Dizirconacyclooctatetraene. *Chemistry – A European Journal* **2018,** *24*, 5667-5674.

[2] Burlakov, V. V.; Beweries, T.; Bogdanov, V. S.; Arndt, P.; Baumann, W.; Petrovskii, P. V.; Spannenberg, A.; Lyssenko, K. A.; Shur, V. B.; Rosenthal, U., Synthesis and Isolation of Di-n-butylhafnocene and Its Application as a Versatile Starting Material for the Synthesis of New Hafnacycles. *Organometallics* **2009,** *28*, 2864–2870.

[3] Fulmer, G. R.; Miller, A. J. M.; Sherden, N. H.; Gottlieb, H. E.; Nudelman, A.; Stoltz, B. M.; Bercaw, J. E.; Goldberg, K. I., NMR Chemical Shifts of Trace Impurities: Common Laboratory Solvents, Organics, and Gases in Deuterated Solvents Relevant to the Organometallic Chemist. *Organometallics* **2010,** *29*, 2176-2179.

[4] Chen, S.; Wang, J.; Wang, H., Synthesis, characterization and pyrolysis of a high zirconium content zirconocene–polycarbosilane precursor without Zr–O bond. *Materials & Design* **2016,** *90*, 84-90.

[5] Sheldrick, G. M. Crystal structure refinement with *SHELXL. Acta Cryst*., 2008, **A64**, 112-122.

[6] Sheldrick, G. M. *SHELXT* - Integrated space-group and crystal-structure determination. *Acta Cryst.*, 2015, **C71**, 3-8.

[7] Diamond - Crystal and Molecular Structure Visualization, Crystal Impact - Dr. H. Putz & Dr. K. Brandenburg GbR, Kreuzherrenstr. 102, 53227 Bonn, Germany, http://www.crystalimpact.com/diamond.

[8] Takahashi, K.; Morishita, H.; Ogiwara, Y.; Sakai, N., Group 4 Metallocene Difluoride/Palladium Bimetallic Catalysts for the Reductive Cross-Coupling of Alkynes with Aryl Iodides and Bromides. *The Journal of Organic Chemistry* **2018,** *83*, 13734-13742.

[9] *Gaussian 16, Revision C.01*, Frisch, M. J.; Trucks, G. W.; Schlegel, H. B.; Scuseria, G. E.; Robb, M. A.; Cheeseman, J. R.; Scalmani, G.; Barone, V.; Petersson, G. A.; Nakatsuji, H.; Li, X.; Caricato, M.; Marenich, A. V.; Bloino, J.; Janesko, B. G.; Gomperts, R.; Mennucci, B.; Hratchian, H. P.; Ortiz, J. V.; Izmaylov, A. F.; Sonnenberg, J. L.; Williams-Young, D.; Ding, F.; Lipparini, F.; Egidi, F.; Goings, J.; Peng, B.; Petrone, A.; Henderson, T.; Ranasinghe, D.; Zakrzewski, V. G.; Gao, J.; Rega, N.; Zheng, G.; Liang, W.; Hada, M.; Ehara, M.; Toyota, K.; Fukuda, R.; Hasegawa, J.; Ishida, M.; Nakajima, T.; Honda, Y.; Kitao, O.; Nakai, H.; Vreven, T.; Throssell, K.; Montgomery, J. A., Jr.; Peralta, J. E.; Ogliaro, F.; Bearpark, M. J.; Heyd, J. J.; Brothers, E. N.; Kudin, K. N.; Staroverov, V. N.; Keith, T. A.; Kobayashi, R.; Normand, J.; Raghavachari, K.; Rendell, A. P.; Burant, J. C.; Iyengar, S. S.; Tomasi, J.; Cossi, M.; Millam, J. M.; Klene, M.; Adamo, C.; Cammi, R.; Ochterski, J. W.; Martin, R. L.; Morokuma, K.; Farkas, O.; Foresman, J. B.; Fox, D. J. Gaussian, Inc., Wallingford CT, **2016**

[10] Reiß, F.; Reiß, M.; Spannenberg, A.; Jiao, H.; Hollmann, D.; Arndt, P.; Rosenthal, U.; Beweries, T., Titanocene Silylpropyne Complexes: Promising Intermediates en route to a Four-Membered 1-Metallacyclobuta-2,3-diene? *Chem. Eur. J.* **2017,** *23*, 14158-14162.

[11] a) Becke, A. D., Density-functional exchange-energy approximation with correct asymptotic behavior. *Phys. Rev. A* **1988**, *38*, 3098–3100; b) Perdew, J. P., Density-functional approximation for the correlation energy of the inhomogeneous electron gas. *Phys. Rev. B* **1986**, *33*, 8822–8824.

[12] a) Vosko, S. H.; Wilk, L.; Nusair, M., Accurate spin-dependent electron liquid correlation energies for local spin density calculations: a critical analysis. *Can. J. Phys.* **1980**, *58*, 1200–1211; b) Lee, C.; Yang, W.; Parr, R. G., Development of the Colle-Salvetti correlation-energy formula into a functional of the electron density. *Phys. Rev. B* **1988**, *37*, 785–789; c) Miehlich, B.; Savin, A.; Stoll, H.; Preuss, H., Results obtained with the correlation energy density functionals of becke and Lee, Yang and Parr. *Chem. Phys. Lett.* **1989**, *157*, 200–206; d) Becke, A. D., Density-functional thermochemistry. III. The role of exact exchange. *J. Chem. Phys.* **1993**, *98*, 5648–5652.

[13] Weigend, F.; Ahlrichs, R. Balanced basis sets of split valence, triple zeta valence and quadruple zeta valence quality for H to Rn: Design and assessment of accuracy. *Phys. Chem. Chem. Phys.* **2005**, *7*, 3297–3305.

[14] a) Grimme, S.; Antony, J.; Ehrlich, S.; Krieg, H., A consistent and accurate ab initio parametrization of density functional dispersion correction (DFT-D) for the 94 elements H-Pu. *J. Chem. Phys.* **2010**, *132*, 154104; b) Grimme, S.; Ehrlich, S.; Goerigk, L., Effect of the damping function in dispersion corrected density functional theory. *J. Comput. Chem.* **2011**, *32*, 1456–1465.

[15] Reiss, F.; Reiss, M.; Bresien, J.; Spannenberg, A.; Jiao, H.; Baumann, W.; Arndt, P.; Beweries, T., 1-Titanacyclobuta-2,3-diene - an elusive four-membered cyclic allene. *Chem. Sci.* **2019,** *10*, 5319-5325.

[16] Marenich, A. V.; Cramer, C. J.; Truhlar, D. G., Universal Solvation Model Based on Solute Electron Density and on a Continuum Model of the Solvent Defined by the Bulk Dielectric Constant and Atomic Surface Tensions. *J. Phys. Chem. B* **2009,** *113*, 6378-6396.